UNIVERSITY OF CALIFORNIA
RIVERSIDE

Nonempirically-Tuned Density Functional Theory Approaches for Accurately Predicting Electron Affinities and Halogen-Bonding Interactions

A Thesis submitted in partial satisfaction
of the requirements for the degree of

Master of Science

in

Chemical and Environmental Engineering

by

Lindsey Anderson

December 2017

Thesis Committee:
Dr. Bryan M. Wong, Chairperson
Dr. Jianzhong Wu
Dr. Ruoxue Yan

The Thesis of Lindsey Anderson is approved:

_____

_____

_____

Committee Chairperson

University of California, Riverside

Acknowledgements

The text of this thesis in Chapter 1, in full, is a reprint of the material as it appears in the *Journal of Chemical Theory and Computation* on March 24, 2017. The co-author Dr. Bryan Wong listed in that publication directed and supervised the research which forms the basis for this thesis. In addition, the co-author M. Belen Oviedo listed in that publication provided additional technical expertise. The text of this thesis in Chapter 2 is pending publication in *Journal of Chemical Theory and Computation* (as of December 4, 2017) and was also directed and supervised by Dr. Bryan Wong. Additionally, Alexandra Raeber and Xi Chen assisted with the initial setup and analysis of the halogen-bonding data and Dr. Fredy Aquino conducted additional calculations and analysis.

We gratefully acknowledge Professor Frank Jensen for providing the computational details and settings required to converge SCF calculations with non-standard, extremely diffuse basis sets. This work was supported by the U.S. Department of Energy, Office of Science, Early Career Research Program under Award No. DE-SC0016269. We acknowledge the National Science Foundation for the use of supercomputing resources through the Extreme Science and Engineering Discovery Environment (XSEDE), Project No. TG- ENG160024.

Table of Contents

OVERALL INTRODUCTION……1

CHAPTER 1: ACCURATE ELECTRON AFFINITIES AND ORBITAL ENERGIES OF ANIONS FROM A NONEMPIRICALLY TUNED RANGE-SEPARATED DENSITY FUNCTIONAL THEORY APPROACH……...3

Abstract……..3

Introduction……4

Methodology……..7

Nonempirically Tuned Range-Separated DFT……7

Non-Standard, Extremely Diffuse Basis Sets……..9

Results and Discussion……11

Conclusions…….26

CHAPTER 2. HALOGEN BONDING INTERACTIONS: REVISED BENCHMARKS AND A NEW ASSESSMENT OF EXCHANGE VS. DISPERSION…….28

Abstract……28

Introduction……..28

Methodology……31

Contributions from Exact Exchange……..35

Contributions from Dispersion……..38

Results and Discussion……40

Contributions from Exact Exchange……..43

Contributions from Dispersion……..47

Conclusions……52

OVERALL CONCLUSIONS……54

REFERENCES……56

APPENDIX A……..66

APPENDIX B……..67

List of Figures

Figure 1, p. 11: Plots of J^2 as a function of μ for all three rows of elements in the periodic table (H-Ar) using (a) the smaller aug-pc-2 and (b) the customized diffuse aug-pc-∞ basis sets.

Figure 2, p. 14: Plot of the spatial extent, $\langle R^2 \rangle$ (expectation value of R^2), for each anion as a function of $1/\mu$ obtained with the customized diffuse aug-pc-∞ basis.

Figure 3, p. 16: Errors in the electron affinity computed via a ΔSCF procedure, EA = E(N) – E(N + 1), for all three rows of elements in the periodic table using the (a) aug-pc-2 and (b) customized diffuse aug-pc-∞ basis sets.

Figure 4, p. 21: Errors in the electron affinity computed from the negative HOMO energy of the anion, $-E_{\mathrm{HOMO}}$, for all three rows of elements in the periodic table using the (a) aug-pc-2 and (b) customized diffuse aug-pc-∞ basis sets.

Figure 5, p. 23: Variation of the electronic energy, E, as a function of electron number, N, applied to the fluorine anion using the (a)-(b) aug-pc-2 and (c)-(d) customized diffuse aug-pc-∞ basis sets. The variation of E vs. N is shown in (a) and (c), whereas the deviation from linearity is shown in (b) and (d).

Figure 6, p. 29: A prototypical halogen bond (XB) in which a halogen atom X (Br) forms a non-covalent bond with a Lewis base B (pyridine).

Figure 7, p. 32: Molecular geometries in the XB18 benchmark set. This set contains all nine combinations of diatomic halogen donors (Br_2, BrI, ClBr, ClI, FBr, FI, HBr, HI, and I_2) with two halogen acceptors (NCH and H_2CO).

Figure 8, p. 34: Molecular geometries in the XB51 benchmark set. This set covers a broad distribution of dissociation energies ranging from the weak FCCH-based dimers to the strongly bonded organometallic $PdHP_2Cl$-based dimers.

Figure 9, p. 42: Plots of J^2 (Eq. 2) as a function of ω for a representative set of halogen bonding dimers.

Figure 10, p. 46: Absolute errors in the dissociation energy predicted by various DFT functionals without dispersion for halogen-bonding dimers within the (a) XB18 and (b and c) XB51 benchmark sets.

Figure 11, p. 49: Absolute errors in the dissociation energy predicted by the standard LC-ωPBE functional (ω = 0.47), with and without dispersion for halogen-bonding dimers within the (a) XB18 and (b and c) XB51 benchmark sets.

Figure 12, p. 51: Root mean square deviation (RMSD) and mean signed error (MSE) for halogen-bonding dissociation energies obtained with various DFT methods.

List of Tables

Table 1, p. 12: Nonempirically-tuned μ values ($Bohr^{-1}$) for all three rows of elements in the periodic table (H-Ar).

Table 2, p. 16: Electron affinities (in eV) computed via a ΔSCF procedure, EA = E(N) – E(N + 1), for all three rows of elements in the periodic table using the aug-pc-2 and customized diffuse aug-pc-∞ basis sets.

Table 3, p. 20: Electron affinities (in eV) computed from the negative HOMO energy of the anion, $-E_{\mathrm{HOMO}}$, for all three rows of elements in the periodic table using the aug-pc-2 and customized diffuse aug-pc-∞ basis sets.

Table 4, p. 41: Revised benchmark dissociation energies (in kcal/mol) for the XB51 set, at the $E_{\mathrm{CBS/MP2(Q5)}}^{\mathrm{CCSD(T)/aVTZ}}$ level of theory.

Table 5, p. 43: Optimal ω values for each halogen-bonding dimer in units of $bohr^{-1}$.

Table 6, p. 47: Mean absolute errors in kcal/mol for halogen-bonding dissociation energies obtained with various DFT methods.

Table 7, p. 51: Mean signed error (MSE), root-mean-square deviation (RMSD), and maximum error for halogen-bonding dissociation energies obtained with various DFT methods.

Overall Introduction

A common situation that arises in theoretical chemistry and physics involves finding an accurate computational method that describes molecular systems, ranging from simple single atoms to complex many-body molecular systems.[1] Many quantum mechanical modelling theories have been developed that attempt to describe the behaviors of electrons within these systems. More specifically, they attempt to provide an approximate solution to the time-independent Schrodinger equation that finds energy levels via the electronic wavefunction.[2] While the Schrodinger equation can be solved for the simplest atom, hydrogen, it is nearly impossible to quantify the complex electronic and nucleic interactions in systems containing more than one electron. The Hartree-Fock (HF) theory provides a simple, yet reasonable approximation to this problem that approximates the *N*-electron wavefunction using a product of *N* one-electron wavefunctions, where the product is known as the Slater determinant.[2]

There are also more-recently developed methods that implement the concepts of HF theory in addition to providing other approximations in an attempt to give a more accurate description of electronic interactions within many-body systems. The main theory focused on in this paper was first introduced in 1964 by Hohenberg and Kohn[3] and further described in 1965 by Kohn and Sham[4] and is known today as density functional theory, or DFT. While this theory took many decades to gain credibility, it is one of the most commonly used molecular theories today and is praised for providing a significantly more accurate description of electronic structures when compared to HF. DFT essentially describes the ground state energy (E_0) of molecular systems based on the electron density

of that system.[5] In other words, DFT uses functionals, or functions of a function, that are based on the number of electrons and their positions in relation to one another to describe ground-state properties like electron affinities and molecular orbital energies. This provides a vast improvement to other post-HF theories that tend to have high computational costs.

One downfall to DFT is that the exact functionals that describe the exchange-correlation energies (E_{xc}) between electrons is not known for systems containing more than a single electron. To fix this, one must approximate this E_{xc} by combining a variety of functionals with an appropriate basis set, which is essentially a finite set of functions composed of atomic orbitals or plane-waves that are used to provide solutions to the Schrodinger equation. In this thesis, an investigation into the accuracy of various DFT functionals and basis sets is provided for select complex molecular systems, namely systems involving anions and halogen-bonding molecules.

Chapter 1: Accurate Electron Affinities and Orbital Energies of Anions from a Nonempirically Tuned Range-Separated Density Functional Theory Approach

Abstract

The treatment of atomic anions with Kohn–Sham density functional theory (DFT) has long been controversial because the highest occupied molecular orbital (HOMO) energy, E_{HOMO}, is often calculated to be positive with most approximate density functionals. We assess the accuracy of orbital energies and electron affinities for all three rows of elements in the periodic table (H–Ar) using a variety of theoretical approaches and customized basis sets. Among all of the theoretical methods studied here, we find that a nonempirically tuned range-separated approach (constructed to satisfy DFT-Koopmans' theorem for the anionic electron system) provides the best accuracy for a variety of basis sets, even for small basis sets where most functionals typically fail. Previous approaches to solve this conundrum of positive E_{HOMO} values have utilized non-self-consistent methods; however, electronic properties, such as electronic couplings/gradients (which require a self-consistent potential and energy), become ill-defined with these approaches. In contrast, the nonempirically tuned range-separated procedure used here yields well-defined electronic couplings/gradients and correct E_{HOMO} values because both the potential and resulting electronic energy are computed self-consistently. Orbital energies and electron affinities are further analyzed in the context of the electronic energy as a function of electronic number (including fractional numbers of electrons) to provide a stringent assessment of self-interaction errors for these complex anion systems.

Introduction:

The quantum mechanical description of weakly-bound anions and their unusual properties continues to garner immense interest in the atomic/molecular physics and condensed-phase chemistry communities. In particular, the weak binding of an extra electron to a stable neutral atom/molecule is central to the study of Rydberg states,[6-8] few-body quantum systems,[9] and their couplings to the electronic continuum.[10-12] Within the rapidly-growing field of condensed-phase chemistry, loosely-bound electrons are present as solvated electrons in which an extra electron is not associated to any one particular molecule but is collectively bound by a cluster of solvent molecules.[13-15] In the broader fields of chemistry and materials science, anions and radicals play a vital role in semiconducting molecular clusters,[16-17] fullerenes,[18-19] charge transfer,[20] and solar cells.[21-22]

To describe these highly complex processes and electronic environments, an accurate quantum mechanical treatment is necessary, and advances in density functional theory (DFT) have enabled first-principles calculations with reasonable accuracy (mean absolute errors around 0.2 eV).[23] However, during the formative stages of DFT in quantum chemistry, serious concerns were raised that Kohn-Sham DFT was not appropriate for the study of anions since the HOMO energy was often calculated to be positive – typically for small basis sets, and surprisingly for atomic species with sizeable electron affinities.[24-28] A positive HOMO eigenvalue is problematic since this implies that the anion is unbound, and the calculation is, in principle, unreliable.[29] At the time, these problematic cases were shown to arise from the deficiency of LDA/GGA exchange-correlation functionals since

Kohn-Sham potentials obtained from these approximations exhibit the wrong asymptotic behavior.[30] Still, other researchers have argued that electron affinities calculated using reasonable basis sets (even with these conventional DFT methods) are still reliable when calculated as a difference between the self-consistent total energies of the anion and neutral species.[31] These controversial issues continue to interest DFT purists, and recent parallel studies by Burke[32] and Jensen[33] have demonstrated that anions which should be bound states in reality are actually described as metastable electronic resonances by many approximate DFT methods. Burke and co-workers[32] have attributed these discrepancies to strong self-interaction errors (SIEs) that arise from a net negative charge, resulting in an effective potential where the last electron is actually unbound.

Numerous publications have appeared using DFT methods to calculate electron affinities[23, 34-36] (including recent developments in extended Koopmans' Theorem approaches[37-39]), and three solutions have been proposed to address the conundrum of positive E_{HOMO} values in Kohn-Sham DFT: (1) Ignore warnings on positive HOMO energies:[23] This viewpoint is a pragmatic approach to simply "march on" and compute electron affinities as energy differences between the anion and neutral species; however, the presence of a formally problematic, positive HOMO energy is unsettling since one "obtains the right answer for the wrong reason"; (2) Use an orbital-dependent self-interaction correction scheme:[40-41] This approach can, in principle, directly eliminate SIE terms in an orbital-by-orbital procedure; however, a detailed study by Scuseria and co-workers[28] has shown that these self-interaction corrections can severely impair equilibrium properties, in addition to introducing computational difficulties due to the invariance of the

energy with respect to unitary transformations; (3) Self-consistently compute orbitals using Hartree-Fock (HF), but use the HF density to non-self-consistently evaluate the energy with DFT:[32, 42] While this most recently proposed approach will formally result in a bound anion with a negative E_{HOMO}, the calculation of electronic properties, such as electronic couplings or gradients, becomes ill-defined since the potential is evaluated with one approach while the energy is non-self-consistently evaluated with another approximation.

In this work, we instead propose the following alternative: use a non-empirically tuned procedure to satisfy DFT-Koopmans' theorem for the anionic (N+1) electron system, and use the resulting tuned XC functional to self-consistently evaluate both orbital energies and electron affinities. This procedure should yield correct E_{HOMO} values and well-defined electronic couplings/gradients since both the potential and resulting electronic energy are computed self-consistently. We test the accuracy of this approach by computing both the orbital energies and electron affinities for all three rows of elements in the periodic table (H-Ar). We have chosen to focus our attention on individual atoms since SIEs are particularly severe for isolated atoms where the extra electron is strongly localized.[43] A variety of theoretical methods and extremely diffuse, customized basis sets are used in this work (containing exponents less than 10^{-10}), which require special modifications to existing codes to achieve convergence at the basis set limit. Finally, we examine the orbital energies and electron affinities in the context of the electronic energy, E, as a function of electronic number, N, including fractional numbers of electrons.[44] These tests of deviations from linearity provide a stringent assessment of SIEs inherent to the underlying functional itself as well as a critical diagnostic of the basis set used in the calculation.[45] We give a detailed

analysis of these *E* vs. *N* curves and discuss the implications of using a non-empirically tuned approach for obtaining accurate and formally-correct bound anions with well-defined electronic properties in a fully self-consistent approach.

Methodology

The main purpose of this work is to (1) assess the accuracy of non-empirically tuned range-separated DFT and (2) understand the effects of non-standard, extremely diffuse basis sets for simultaneously computing electron affinities and orbital energies for anions– both of which are briefly reviewed here.

Non-Empirically Tuned Range-Separated DFT: In contrast to conventional hybrid functionals, the range-separated formalism[24, 25] mixes short range density functional exchange with long range HF exchange by partitioning the electron repulsion operator into short and long range terms (i.e., the mixing parameter is a function of electron coordinates):

$$\frac{1}{r_{12}} = \frac{1-\mathrm{erf}\left(\mu \cdot r_{12}\right)}{r_{12}} + \frac{\mathrm{erf}\left(\mu \cdot r_{12}\right)}{r_{12}}. \qquad (1)$$

The erf term denotes the standard error function, r_{12} is the interelectronic distance between electrons 1 and 2, and μ is the range-separation parameter in units of Bohr^{-1}. The second term in Eq. (1) is of particular importance since it enforces a rigorously correct 100% contribution of asymptotic HF exchange, which we[46-50] and others[51-52] have found to be essential for accurately describing long-range charge-transfer excitations, orbital energies, and valence excitations in even relatively simple molecular systems. For pure density functionals (such as the generalized gradient BLYP used here or the PBE kernel) which do

not already include a fraction of nonlocal HF exchange, the exchange-correlation (XC) energy within the range-separated formalism is

$$E_{xc}(\mu) = E_{c,\mathrm{DFT}}(\mu) + E_{x,\mathrm{DFT}}^{\mathrm{SR}}(\mu) + E_{x,\mathrm{HF}}^{\mathrm{LR}}(\mu). \quad (2)$$

$E_{c,\mathrm{DFT}}$ is the DFT correlation functional, $E_{x,\mathrm{DFT}}^{\mathrm{SR}}$ is the short-range DFT exchange functional, and $E_{x,\mathrm{HF}}^{\mathrm{LR}}$ is the HF contribution to exchange computed with the long-range part of the Coulomb operator. Baer and Kronik[53-54] have shown that the range-separation parameter, μ, is system dependent but can be non-empirically tuned to satisfy DFT-Koopmans' theorem.[55-57] In summary, this theorem states that the HOMO energy equals the negative of the ionization potential (IP); the latter is typically obtained from the difference of two separate energy calculations via a ΔSCF procedure. Within the Kohn-Sham DFT formalism, this condition is fulfilled for the exact XC-functional; therefore, adjusting the range-separation parameter in this self-consistent manner provides a theoretical justification for this procedure. While the original non-empirical tuning procedure focused on computing the HOMO and IP for neutral systems, we have slightly modified this procedure to non-empirically compute electron affinities and orbital energies of anions by minimizing the following objective function:

$$J^2(\mu) = \left[\varepsilon_{\mathrm{HOMO}}^{\mu}(N+1) + \mathrm{EA}^{\mu}(N)\right]^2, \quad (3)$$

where $\varepsilon_{\mathrm{HOMO}}^{\mu}(N+1)$ is the HOMO energy of the *anionic* (N+1)-electron system and $\mathrm{EA}^{\mu}(N)$ is the electron affinity computed via a ΔSCF energy difference between the N and N+1 electron systems with the same range-separation parameter:

$\mathrm{EA}^{\mu}(N) = E^{\mu}(N) - E^{\mu}(N+1)$. Note that the electron affinity, $\mathrm{EA}^{\mu}(N)$, used in this work is defined as a positive number, which is the same convention used by Jensen,[33] Burke,[32] and Tozer[45] in their previous studies of electron affinities. It should also be noted that with this definition, the electron affinity of the *N*-electron system is equal to the IP of the (*N* + 1)-electron system (i.e. $\mathrm{EA}^{\mu}(N) = \mathrm{IP}^{\mu}(N+1)$), so the objective function in Eq. (3) is a non-empirical approach to satisfy DFT-Koopmans' theorem for anions. To obtain the optimal μ values for each oligomer, several single-point energy calculations for each of the individual anions were carried out by varying μ from 0.1 to 0.6 (in increments of 0.05) for each of the *N* and *N* – 1 electron states. The objective function, J^2 (Eq. 3), was computed as a function of μ for each anion, and spline interpolation was subsequently used to refine the minimum for each individual system.

Non-Standard, Extremely Diffuse Basis Sets: Throughout this work, we compare two basis sets for computing the electron affinities and orbital energies in atomic anions: a conventional aug-pc-2 basis[58] (a triple-zeta quality basis augmented with diffuse functions) and a customized diffuse basis set which we denote as aug-pc-∞. Following the same approach as Jensen,[33] this customized aug-pc-∞ basis set was constructed by adding both diffuse *s*- and *p*- functions to the aug-pc-4 basis by scaling the outer exponent in a geometric progression with a factor of $\sqrt{10}$ until the exponent of the most diffuse function became less than 10^{-10}. Furthermore, we have used the aug-pc-2 and aug-pc-∞ basis sets in their uncontracted forms to avoid any possible contraction errors. The uncontracted basis sets for all the anions are listed in the Supporting Information for completeness. As demonstrated by Jensen,[33] calculations with extremely diffuse basis functions of this

magnitude pose a variety of numerical issues that standard settings in many computational chemistry codes are not capable of handling. As such, all calculations were carried out with a locally modified version of the Gaussian 09 package[59] specifically tailored to handle these non-standard, extremely diffuse basis sets. Specifically, all integral thresholds were tightened to machine precision and density matrices were converged to at least 10^{-8}. The XC potential was calculated using an extremely dense Euler-Maclaurin radial grid[60] with 5000 points in combination with a Lebedev angular grid with 434 points by setting int(acc2e=20,grid=5000434) in the Gaussian route section. Previous work by Jensen[33] has shown that these large radial and angular grids are necessary for numerical integration involving basis functions having small exponents such that the Davidson radial norm criterion is fulfilled to within 10^{-6}. In addition, threshold screenings for discarding integration points with low density were disabled by changing the constant SmlExp from 1.0d-6 to 1.0d-15 in the Gaussian routines utilnz.F and l301.F. Most importantly, we[61] and others[33] have found that XC-functionals containing a large percentage of exact exchange can converge to saddle points in the electronic parameter space, especially when near-degenerate orbitals are present[61] or when extremely diffuse basis sets are used.[33] As such, all SCF solutions were verified to be genuine minima in the electronic parameter space by carrying out a stability analysis to converge (if possible) toward a lower-energy broken-symmetry solution (by setting both scf(qc,conver=9) and stable=opt in the Gaussian route section), which allows for an unrestricted spin state as well as a reduction in symmetry of the orbitals.

Results and Discussion

Figure 1 shows the smooth curves that result from computing J^2 as a function of μ for the first three rows of elements in the periodic table (H – Ar). The upper panel (a) in Figure 1 depicts the J^2 plots using the smaller aug-pc-2 basis, and the lower panel (b) shows the corresponding plots for the same atoms with the customized diffuse aug-pc-∞ basis. The optimally-tuned μ values for all anions obtained with both basis sets are summarized in Table 1.

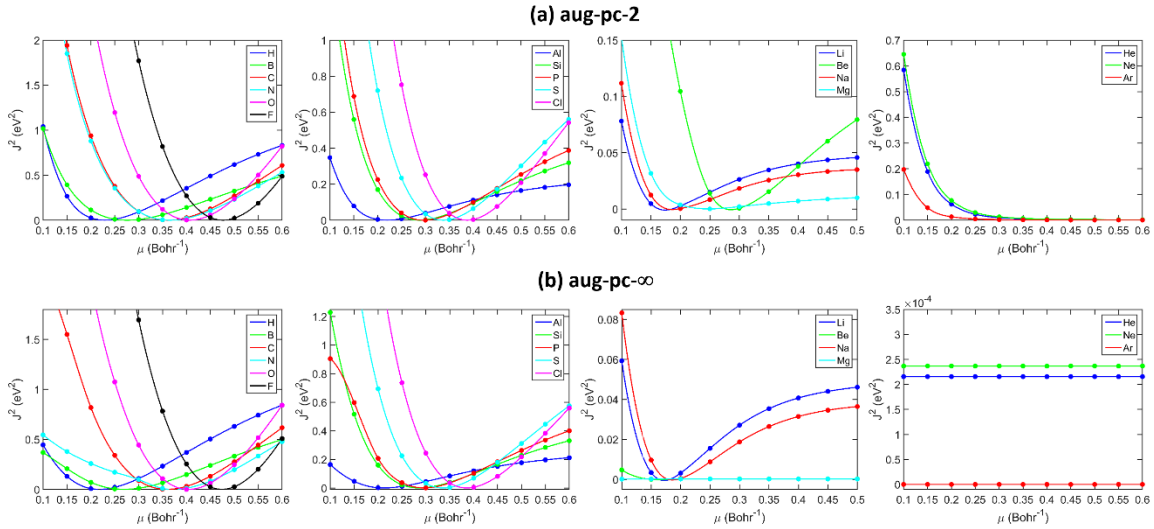

Figure 1. Plots of J^2 as a function of μ for all three rows of elements in the periodic table (H-Ar) using (a) the smaller aug-pc-2 and (b) the customized diffuse aug-pc-∞ basis sets.

Table 1. Nonempirically-tuned μ values ($Bohr^{-1}$) for all three rows of elements in the periodic table (H-Ar).

Anion	aug-pc-2	aug-pc-∞	Anion	aug-pc-2	aug-pc-∞
H	0.22939	0.21759	Ne	–	–
He	–	–	Na	0.18633	0.18614
Li	0.17396	0.17209	Mg	0.24821	–
Be	0.28572	–	Al	0.21966	0.21218
B	0.27586	0.26903	Si	0.28778	0.28643
C	0.36178	0.35958	P	0.29623	0.29661
N	0.36519	0.37228	S	0.33761	0.33593
O	0.40676	0.40425	Cl	0.38736	0.38556
F	0.47631	0.47418	Ar	–	–

Based on the tabulated values of μ and their corresponding plots in Fig. 1, it is interesting to note that increasing the diffuseness of the basis set has a negligible effect (less than 1%) on the non-empirically tuned range-separated parameter. Minor exceptions to this trend include the Be and Mg atoms which exhibit J^2 minima for the smaller aug-pc-2 basis but show nearly flat lines for the customized diffuse aug-pc-∞ basis. This discrepancy arises since the Be and Mg atoms have a closed shell electronic configuration, and the addition of an extra electron leads to a strong inter-electronic repulsion. As such, the customized diffuse aug-pc-∞ basis possesses enough flexibility to allow the extra electron to drift off to infinity (discussed further at the end of this section), whereas the extra electron in the smaller aug-pc-2 basis is artificially confined to remain close to the nucleus. It should also be noted that both the aug-pc-2 and aug-pc-∞ basis do not exhibit J^2 minima for any of the noble gas atoms (He, Ne, and Ar) as both basis sets correctly predict these anions to be unbound. To further understand the sensitivity of our results to the range-separation parameter, μ, we carried out a series of benchmark tests, presented in full detail in the Supporting Information. In short, we also investigated the more

commonly-used IP-tuning procedure by minimizing the following objective function: $J^2(\mu) = \left[\varepsilon^{\mu}_{\mathrm{HOMO}}(N) + \mathrm{IP}^{\mu}(N) \right]^2$, where $\varepsilon^{\mu}_{\mathrm{HOMO}}(N)$ is the HOMO energy of the neutral N-electron system and $\mathrm{IP}^{\mu}(N)$ is the ionization potential computed via a ΔSCF energy difference between the N-1 and N electron systems. With this common tuning procedure, Fig. SI-1 in the Supporting Information shows that the resulting J^2 plots are qualitatively different than the curves shown in Fig. 1 within the main text. In particular, the optimal μ values obtained with the IP-tuning procedure are larger ($\mu \sim 0.5$) than the corresponding μ values obtained with the EA-tuning procedure in Eq. (3). As a result, these benchmark results support our rationale for using the objective function in Eq. (3) for accurately calculating electron affinities, as opposed to the more commonly-used IP-tuning procedure typically used for neutral systems.

Finally, before we compare these results to other XC functionals, it is worth noting that the short-range DFT exchange in Eq. (2) decays exponentially on a length scale of ~$1/\mu$ and, therefore, smaller non-empirically tuned μ values are associated with larger systems (i.e., a smaller value of μ enables the short-range Coulomb operator to fully decay to zero on the length scale of the system). To demonstrate this trend, we plot the spatial extent, $\langle R^2 \rangle$ (i.e., the expectation value of R^2), for each anion as a function of $1/\mu$ obtained with the extremely diffuse aug-pc-∞ basis (the $\langle R^2 \rangle$ vs. $1/\mu$ plot obtained with the smaller aug-pc-2 basis is similar and is given in the Supporting Information). Indeed, the optimal μ values generally reflect these trends and follow a nearly linear behavior (with the

exception of the small H^- anion) with the larger-sized anions having smaller values of μ than smaller anions.

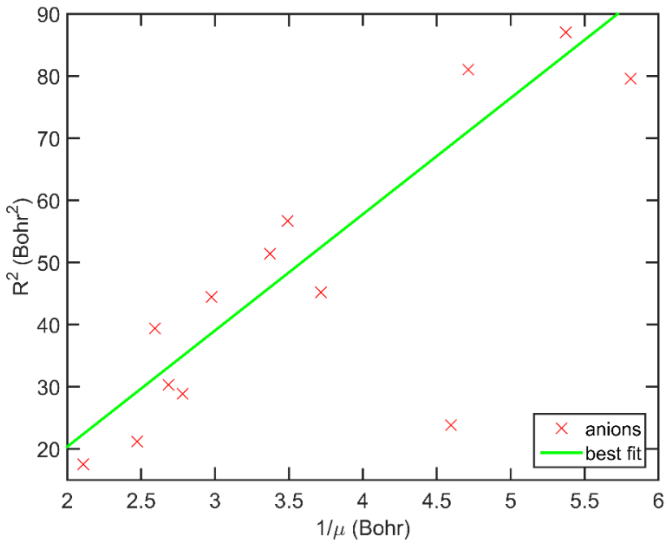

Figure 2. Plot of the spatial extent, $<R^2>$ (expectation value of R^2), for each anion as a function of $1/\mu$ obtained with the customized diffuse aug-pc-∞ basis. The outlier value near $1/\mu = 0.46$ (which corresponds to the H^- anion) was excluded when creating the best fit line.

Turning our attention to previous reports of unbound anions and anomalous orbital energies in conventional XC functionals, we compare our non-empirically tuned results to electron affinities and HOMO energies obtained with the BLYP, B3LYP, BHHLYP, and HF approaches. We have chosen these specific methods for comparison due to their widespread use in previous findings[32-33] and also because they represent different extremes of global hybrids where the HF exchange contribution ranges from 0.20 to 1.00. For example, the pure BLYP functional contains no HF exchange, the popular B3LYP hybrid functional is parameterized with 20% exchange, the half-and-half BHHLYP functional is constructed with 50% exchange, and the HF method is defined with 100% exchange.

Moreover, a comparison of these XC functionals allows a fair and consistent evaluation since all of the DFT methods have similar LYP correlation[62] portions. It is worth noting that we also obtained similar results with other range-separated functionals such as LC-BOP, LC-PBE, and LC-ωPBE, which is consistent with previous work by us[47-49] and Jensen[33] indicating that the long-range $E_{x,\mathrm{HF}}^{\mathrm{LR}}$ exchange term in Eq. (2) plays a more dominant role compared to either $E_{c,\mathrm{DFT}}$ or $E_{x,\mathrm{DFT}}^{\mathrm{SR}}$ in these systems. We do not consider the heavily-parameterized Minnesota functionals in our study since the emphasis of this work is on non-empirically tuned functionals, and very recent reports have shown that most of the Minnesota functionals do not obey rigorously known constraints of the exact functional.[63-64] Table 2 summarizes the electron affinities computed via a ΔSCF procedure (using the same EA = $E(N) - E(N+1)$ expression defined in the Theory and Methodology section) for the first three rows of elements in the periodic table. Total energies calculated with BLYP, B3LYP, BHHLYP, HF, and LC-BLYP for all three rows of elements in the periodic table are given in the Supporting Information. We emphasize that these non-standard calculations were incredibly difficult to converge, and the same integral thresholds, grid sizes, and computational settings described in the Theory and Methodology section were used. In addition, all SCF solutions were verified to be genuine minima in the electronic parameter space by carrying out a stability analysis to converge toward a lower-energy broken-symmetry solution.[61] Electron affinities for all of the noble gas atoms (He, Ne, and Ar) computed with the smaller aug-pc-2 basis were not included since these basis sets are unable to describe these unbound anions. Fig. 3 presents a graphical analysis of Table 2 by plotting the corresponding error ($\mathrm{EA} - \mathrm{EA}_{\mathrm{expt.}}$) in the electron affinity.

Table 2. Electron affinities (in eV) computed via a ΔSCF procedure, EA = E(N) – E(N + 1), for all three rows of elements in the periodic table using the aug-pc-2 and customized diffuse aug-pc-∞ basis sets.

		HF		BLYP		B3LYP		BHHLYP		LC-BLYP	
	EA_{expt}[a]	aug-pc-2	aug-pc-∞	aug-pc-2	aug-pc-∞	aug-pc-2	aug-pc-∞	aug-pc-2	aug-pc-∞	aug-pc-2	aug-pc-∞
H^-	0.75	-0.28	-0.33	0.85	1.21	0.91	1.09	0.67	0.71	0.83	0.84
He^-	0.00	–	0.00	–	0.08	–	0.07	–	0.02	–	0.01
Li^-	0.62	-0.06	-0.03	0.45	0.65	0.55	0.65	0.43	0.46	0.50	0.50
Be^-	0.00	-0.97	-0.01	-0.62	0.38	-0.53	0.29	-0.69	0.07	-0.61	0.02
B^-	0.28	-0.30	-0.30	0.46	0.92	0.47	0.76	0.18	0.35	0.42	0.43
C^-	1.26	0.46	0.45	1.37	1.72	1.38	1.53	1.04	1.03	1.39	1.39
N^-	0.00	-1.64	0.00	0.40	1.14	0.25	0.81	-0.25	0.23	0.23	0.23
O^-	1.46	-0.55	-0.57	1.85	2.22	1.70	1.85	1.13	1.11	1.83	1.83
F^-	3.40	1.21	1.17	3.70	3.80	3.55	3.53	2.92	2.90	3.76	3.74
Ne^-	0.00	–	0.00	–	0.11	–	0.09	–	0.02	–	0.02
Na^-	0.55	-0.05	-0.05	0.49	0.69	0.58	0.67	0.45	0.47	0.53	0.53
Mg^-	0.00	-0.58	0.00	-0.42	0.23	-0.31	0.19	-0.45	0.05	-0.45	0.01
Al^-	0.43	0.03	0.01	0.39	0.71	0.47	0.65	0.28	0.36	0.35	0.36
Si^-	1.39	0.87	0.85	1.24	1.43	1.35	1.40	1.16	1.15	1.26	1.25
P^-	0.75	-0.32	-0.32	0.91	1.24	0.97	1.13	0.72	0.74	0.90	0.90
S^-	2.08	0.90	0.88	2.14	2.25	2.21	2.21	1.96	1.95	2.19	2.19
Cl^-	3.61	2.39	2.37	3.58	3.58	3.68	3.67	3.44	3.42	3.68	3.67
Ar^-	0.00	–	0.00	–	0.11	–	0.09	–	0.02	–	0.00
MAE[b]	–	1.03	0.69	0.21	0.33	0.17	0.23	0.24	0.14	0.20	0.11

[a]Experimental electron affinities from References [65-67]. [b]Mean Absolute Errors relative to experimental electron affinities.

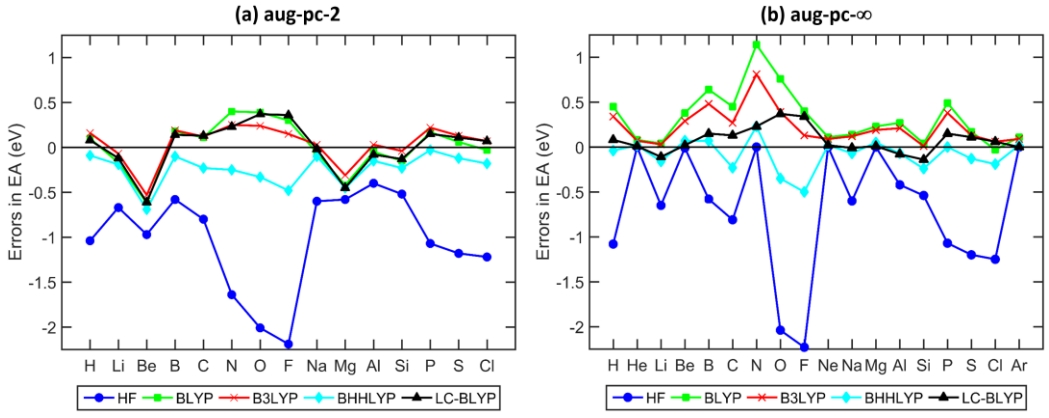

Figure 3. Errors in the electron affinity computed via a ΔSCF procedure, EA = E(N) – E(N + 1), for all three rows of elements in the periodic table using the (a) aug-pc-2 and (b) customized diffuse aug-pc-∞ basis sets.

Based on the tabulated mean absolute errors (MAE) for the customized aug-pc-∞ basis set, the non-empirically tuned LC-BLYP functional gives the best prediction of the ΔSCF electron affinities with a MAE of 0.11 eV, followed by the BHHLYP and B3LYP functionals with MAEs of 0.14 and 0.23 eV, respectively. The pure BLYP functional yields a larger MAE of 0.33 eV as this method does not contain any nonlocal exchange, whereas the HF method significantly underestimates electron affinities for several atoms (cf. Fig. 3), resulting in an even larger MAE of 0.69 eV due to its lack of explicit electron correlation. For all levels of theory and basis sets examined in this work, the largest errors in ΔSCF-computed electron affinities were observed in the halogen atoms (F and Cl) which arise from the strong electron repulsion that the extra electron feels when it is added to a nearly complete *p*-shell. In general, both Table 2 and Fig. 3 clearly demonstrate that XC functionals containing a larger percentage of HF exchange yield the most accurate electron affinities; however, there is an intricate balance between exchange and correlation, and incorporating only 100% nonlocal exchange without correlation as in the HF method (or conversely, neglecting nonlocal exchange completely as in the pure BLYP functional) can severely corrupt the prediction of electron affinities.

We now turn our attention to the central issue of unbound anions and positive HOMO energies originally mentioned in the Introduction. Table 3 summarizes the electron affinities computed from the negative HOMO energy of the anion, $-E_{\mathrm{HOMO}}$ for the first three rows of elements in the periodic table. Again, electron affinities for all of the noble gas atoms (He, Ne, and Ar) computed with the smaller aug-pc-2 basis were not included since these basis sets are unable to describe these unbound anions. Fig. 4 presents a

graphical analysis of Table 3 by plotting the corresponding error ($-E_{HOMO} - EA_{expt.}$) in the electron affinity. It is interesting to note that while the plots in Figs. 3 and 4 were calculated using two different metrics (ΔSCF vs. $-E_{HOMO}$), the resulting plots obtained with the LC-BLYP functional are nearly identical since the non-empirically tuned approach was constructed to satisfy the constraint in Eq. (3) as closely as possible. As mentioned in the Introduction, the sign of E_{HOMO} for anions is a more stringent test of these XC functionals since a positive E_{HOMO} implies that the anion is formally unbound. As clearly shown in Table 3, the non-empirically tuned LC-BLYP functional correctly predicts negative E_{HOMO} values for both basis sets (note that Table 3 lists $-E_{HOMO}$ values) and for all anions, with the exception of the Be, Mg, and noble gas atoms – all of which *are* experimentally unbound. To highlight the robustness of these LC-BLYP results, we also carried out two benchmark tests in the Supporting Information to (1) ascertain the effect of using other basis sets and (2) compare electron affinities obtained with a *fixed* value of μ against the non-empirically tuned LC-BLYP results listed in Table 3. Tables SI-1 and SI-2 in the Supporting Information give the total energies and electron affinities calculated with the LC-BLYP functional (fixed at $\mu = 0.3$) for all three rows of elements in the periodic table using the aug-cc-pVTZ, aug-pc-2, and customized diffuse aug-pc-∞ basis sets. We have chosen $\mu = 0.3$ for our benchmark tests since 0.3 is the numerical average of the μ values listed in Table 1 for all three rows of elements in the periodic table (H-Ar). As demonstrated by the total energies in Table SI-1, Jensen's aug-pc-2 basis set is marginally better than Dunning's triple-zeta aug-cc-pVTZ basis, with the aug-pc-2 basis providing slightly lower total energies across the board. Interestingly, our benchmark test in Table SI-2

demonstrates that the electron affinities calculated with a single value of μ (= 0.3) exhibit impressively low MAE values that are only marginally worse (~ 0.04 eV larger in error) than the non-empirically tuned LC-BLYP results. Most importantly, the LC-BLYP results (fixed at μ = 0.3) are still considerably more accurate than the electron affinities obtained from the other conventional functionals. To further demonstrate the applicability of this approach beyond single atoms, we have also calculated the electron affinities of molecules in the G2-1 data set, which was previously examined in a communication by Burke and co-workers.[42] Table SI-3 in the Supporting Information lists $-E_{HOMO}$ for molecular anions in the G2-1 set computed with the BLYP, B3LYP, BHHLYP, HF, and LC-BLYP approaches. In agreement with previous work by Burke and co-workers,[42] most molecular species (except Cl_2) are predicted to have positive E_{HOMO} values with conventional DFT methods (i.e., BLYP, B3LYP, and BHHLYP), indicating an incorrect unbound nature with these functionals. Only HF and LC-BLYP correctly predict negative E_{HOMO} values in Table SI-3; however, the HF values are significantly overestimated, resulting in a large MAE of 0.73 eV. In contrast, the LC-BLYP functional gives the lowest MAE of 0.29 eV and correctly predicts negative E_{HOMO} values for all molecular species, which highlights the robustness of the range-separation approach in general. Returning to our original discussion on non-empirically tuned approaches for atoms, it should be noted that while the other functionals also give negative E_{HOMO} values in Table 3 for the extremely diffuse aug-pc-∞ basis, their mean absolute errors are still significantly higher than the non-empirically tuned LC-BLYP (MAE = 0.12 eV) functional: HF has a MAE of 0.31 eV, followed by the BHHLYP and B3LYP functionals with MAEs of 0.62 and 0.87 eV. The

pure BLYP functional exhibits the largest MAE of 0.92 eV when the aug-pc-∞ basis is used since almost all of the anions predicted by this functional are unbound or nearly unbound.

Table 3. Electron affinities (in eV) computed from the negative HOMO energy of the anion, $-E_{HOMO}$, for all three rows of elements in the periodic table using the aug-pc-2 and customized diffuse aug-pc-∞ basis sets.

		HF		BLYP		B3LYP		BHHLYP		LC-BLYP	
	EA_{expt}[a]	aug-pc-2	aug-pc-∞	aug-pc-2	aug-pc-∞	aug-pc-2	aug-pc-∞	aug-pc-2	aug-pc-∞	aug-pc-2	aug-pc-∞
H^-	0.75	-0.07	1.26	-1.76	0.02	-1.00	0.01	-0.11	0.01	0.83	0.84
He^-	0.00	–	0.00	–	0.02	–	0.01	–	0.01	–	0.03
Li^-	0.62	0.62	0.67	-1.02	0.00	-0.59	0.00	-0.21	0.00	0.50	0.50
Be^-	0.00	-0.49	0.00	-2.48	0.01	-2.36	0.00	-1.73	0.00	-0.62	0.03
B^-	0.28	0.77	0.78	-1.83	0.03	-1.28	0.02	-0.62	0.01	0.42	0.43
C^-	1.26	2.12	2.13	-1.98	0.01	-1.10	0.01	-0.01	0.01	1.39	1.39
N^-	0.00[a]	-1.46	0.00	-2.95	0.00	-2.22	0.00	-1.39	0.00	0.23	0.23
O^-	1.46	2.19	2.17	-2.35	0.00	-1.26	0.00	0.19	0.21	1.83	1.83
F^-	3.40	4.93	4.92	-1.43	0.01	0.02	0.05	1.97	1.97	3.76	3.74
Ne^-	0.00	–	0.00	–	0.03	–	0.02	–	0.01	–	0.03
Na^-	0.55	0.56	0.58	-1.02	0.00	-0.59	0.00	-0.21	0.00	0.52	0.53
Mg^-	0.00	-0.42	0.00	-1.89	0.04	-1.49	0.03	-1.16	0.02	-0.45	0.03
Al^-	0.43	0.60	0.61	-1.40	0.01	-0.93	0.00	-0.45	0.00	0.35	0.36
Si^-	1.39	1.69	1.69	-1.31	0.01	-0.61	0.01	0.17	0.17	1.26	1.25
P^-	0.75	0.64	0.63	-1.79	0.00	-1.09	0.00	-0.29	0.00	0.90	0.91
S^-	2.08	2.32	2.33	-1.17	0.00	-0.26	0.00	0.84	0.84	2.19	2.18
Cl^-	3.61	4.09	4.09	-0.33	0.00	0.79	0.79	2.17	2.17	3.68	3.67
Ar^-	0.00	–	0.00	–	0.00	–	0.00	–	0.00	–	0.00
MAE[b]	–	0.54	0.31	2.75	0.92	2.04	0.87	1.16	0.62	0.20	0.12

[a] Experimental electron affinities from References [65-67]. [b] Mean Absolute Errors relative to experimental electron affinities.

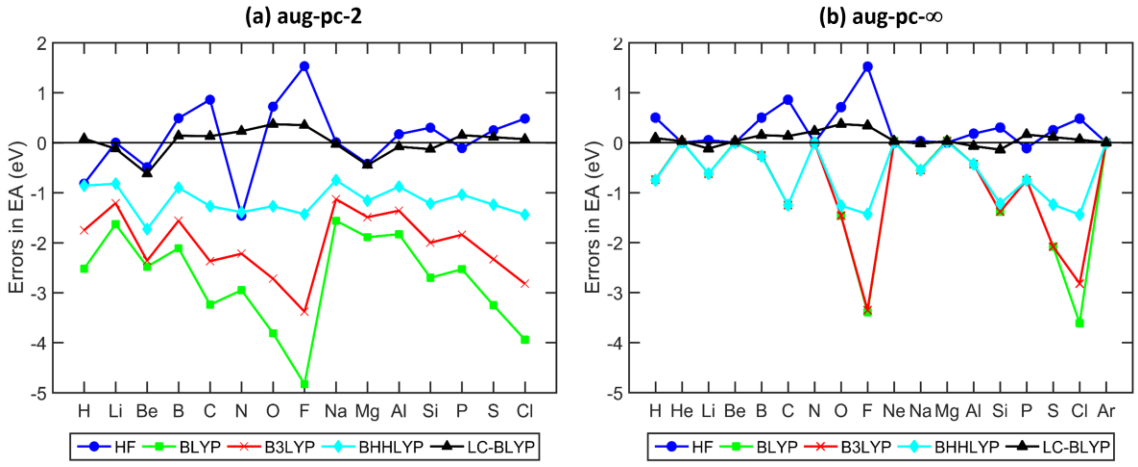

Figure 4. Errors in the electron affinity computed from the negative HOMO energy of the anion, $-E_{HOMO}$, for all three rows of elements in the periodic table using the (a) aug-pc-2 and (b) customized diffuse aug-pc-∞ basis sets.

In stark contrast to the qualitatively good trends obtained with the aug-pc-∞ basis, we encounter particularly worrisome results for the conventional XC functionals when the smaller aug-pc-2 basis is used. While the non-empirically tuned LC-BLYP functional correctly gives negative E_{HOMO} values for both basis sets, the majority of the aug-pc-2 E_{HOMO} values predicted by all other DFT (not including HF) functionals are positive, incorrectly implying that these anions are formally unbound. These positive E_{HOMO} values severely affect their accuracy, resulting in MAEs ranging from 1.16 eV (BHHLYP) to as high as 2.75 eV (BLYP) for the smaller aug-pc-2 basis set. While the purely nonlocal HF method does give negative E_{HOMO} values, the MAEs obtained with this approach are nearly twice that of the non-empirically tuned LC-BLYP approach. Recognizing that the HF method correctly gives negative E_{HOMO} values, Burke and co-workers[32] recently proposed the following solution to compute electron affinities: compute the orbitals using HF (where E_{HOMO} is correctly predicted to be negative) but use the HF density to non-self-consistently

evaluate the energy with an XC potential that contains both exchange and correlation. While this procedure will formally give a properly bound anion with a negative E_{HOMO}, various complications naturally arise: the calculation of electronic gradients becomes ill-defined since the electronic potential is evaluated with one approach while the energy is non-self-consistently evaluated with another approximation. Instead, we propose the following alternative: use a non-empirically tuned procedure (such as Eq. (3)) to satisfy DFT-Koopmans' theorem for the anionic (N+1) electron system, and use the resulting tuned XC functional to self-consistently evaluate both orbital energies and electron affinities. As a result, this procedure should yield correct E_{HOMO} values and well-defined electronic gradients since both the potential and resulting electronic energy are computed self-consistently.

Finally, to complete our analysis of orbital energies and electron affinities of anions, we present a deeper analysis of the electronic energy as a function of electronic number (including fractional numbers of electrons). For an exact functional, Janak proved that E is a piecewise linear function of N, with derivative discontinuities at integer number of electrons.[44] As such, a test of this deviation from linearity provides a stringent assessment of self-interaction errors inherent to the underlying functional itself as well as a diagnostic analysis of the basis set used in the calculation, as pointed out by a recent study by Tozer and co-workers[45] (discussed at the end of this section). Fig. 5 plots the variation of the electronic energy, E, as a function of electron number, N, for one piece of the $E(N)$ curve applied to the fluorine atom using the aug-pc-2 and customized aug-pc-∞ basis sets. Both the variation of E vs. N, (a) and (c), as well as the deviation from linearity, (b) and

(d), are also shown in Fig. 5. We have chosen to focus on fluorine since there have been strong discussions about this anion in several previous studies;[29, 31, 45] however, the main qualitative results discussed in this section equally apply to the other atomic anions.

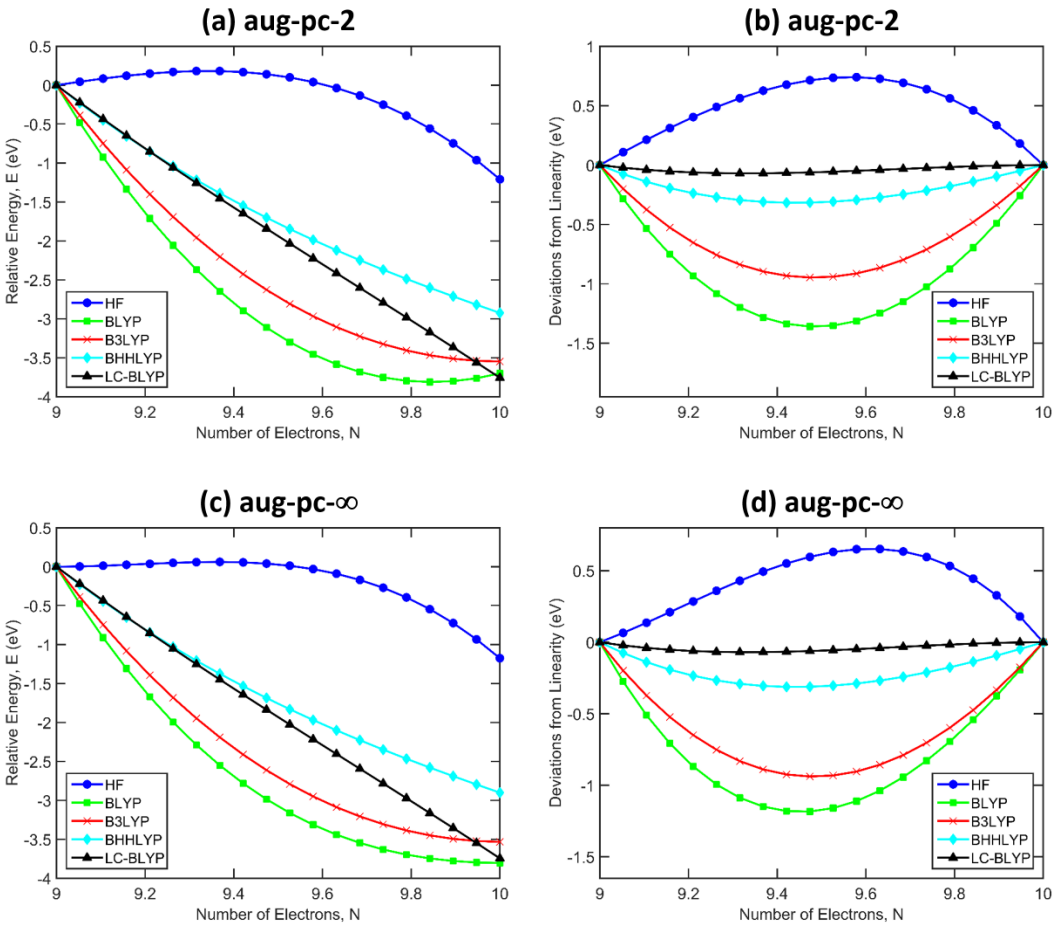

Figure 5. Variation of the electronic energy, *E*, as a function of electron number, *N*, applied to the fluorine anion using the (a)-(b) aug-pc-2 and (c)-(d) customized diffuse aug-pc-∞ basis sets. The variation of *E* vs. *N* is shown in (a) and (c), whereas the deviation from linearity is shown in (b) and (d). The nearly-exact straight line obtained with the non-empirically tuned LC-BLYP functional (for all plots (a)-(d)) implies that this method is nearly SIE-free for the fluorine anion.

As expected, the HF method yields a concave $E(N)$ curve and an energetic destabilization at fractional charges. In contrast, the pure BLYP and hybrid B3LYP/BHHLYP functionals tend to overdelocalize the anion, leading to a convex $E(N)$

curve and an over-stabilization (i.e. a lower energy) of the system at fractional charges. The non-empirically tuned LC-BLYP functional yields a nearly-exact straight line as a function of the fractional charge in the system (cf. Figs. 5(a) and (c)). Furthermore, plots of the deviation from linearity in Figs. 5(b) and (d) imply that the non-empirically tuned LC-BLYP is nearly SIE-free for the fluorine anion.

As we conclude this discussion, it is worth mentioning a few subtle points concerning basis sets that can be seen in Figs. (a) and (c), which were recently discussed in a study by Tozer and co-workers.[45] For any functional, Janak proved that the slope of the $E(N)$ curve at integer number of electrons is related to the orbital energies. Specifically, the limiting value of $\partial E/\partial N$ to the left of an integer M is the HOMO energy, $\varepsilon_{\mathrm{HOMO}}(M)$:

$$\lim_{\delta \to 0} \left. \frac{\partial E}{\partial N} \right|_{N=M-\delta} = \varepsilon_{\mathrm{HOMO}}(M), \tag{4}$$

and the limiting value of $\partial E/\partial N$ to the right of an integer M is the LUMO energy, $\varepsilon_{\mathrm{LUMO}}(M)$:

$$\lim_{\delta \to 0} \left. \frac{\partial E}{\partial N} \right|_{N=M+\delta} = \varepsilon_{\mathrm{LUMO}}(M). \tag{5}$$

For the case of the fluorine system shown in Fig. 5, the $N = 9$ endpoint corresponds to the electron number of the neutral fluorine atom, and $N = 10$ is the electron number of the anion. Fig. 5(a) shows that the limiting value of $\partial E/\partial N$ to the left of $N = 10$ for the BLYP functional is slightly positive; consequently Eq. (4) states that the HOMO energy of the fluorine anion is also positive at the BLYP/aug-pc-2 level of theory, and the anion is formally unbound. However, the $E(N)$ curve for BLYP also possesses a shallow minimum

at $N = 9.85$ in Fig. 5(a), and the energy of the fluorine anion could, in principle, be further stabilized by reducing the electron number to $N = 9.85$ with the remaining 0.15 fraction of an electron drifting off to infinity with zero energy. As pointed out by Tozer and co-workers,[45] the use of a small basis set prevents this from happening since all of the electrons are artificially confined to remain close to the nucleus. However, if the basis was sufficiently augmented with diffuse functions to enable fractional electron loss, the $E(N)$ curve would approach an idealized flattening and give $\varepsilon_{\mathrm{HOMO}} = 0$ according to Eq. (4). Indeed, we do observe an idealized flattening of the $E(N)$ curve for the BLYP functional in Fig. 5(c), leading to a nearly zero $\varepsilon_{\mathrm{HOMO}}$ value (cf. Table 3) when the aug-pc-∞ basis is utilized. This same assessment, in regards to the flattening of the $E(N)$ curve, can also be applied to the numerical BLYP results in Table 2, where the electron affinities computed via the ΔSCF procedure are observed to increase when the aug-pc-2 basis is systematically increased towards the larger aug-pc-∞ basis set. Using a similar analysis for concave behavior, the $E(N)$ curve for HF possesses a shallow maximum at $N = 9.35$ in Fig. 5(a), and the system could, in principle, lower its energy by reducing the electron number in that vicinity to $N = 9$; however, a small basis set again prevents this. When the extremely diffuse aug-pc-∞ basis is used, the HF curve flattens near $N = 9$ and approaches the idealized behavior described by Tozer and co-workers. With this analysis, we now point out that the non-empirically tuned LC-BLYP functional does not exhibit any tendency towards a flattening or fractional electron loss (similar to the CAM-B3LYP analyses in Ref. [45]), resulting in an accurate fluorine orbital energy/electron affinity and a correctly bound anion for both basis sets.

Conclusions

In this study, we have assessed the accuracy of orbital energies and electron affinities for all three rows of elements in the periodic table (H-Ar) using a variety of theoretical approaches and customized basis sets. Specifically, we have closely examined the electron affinities of these anions using two different metrics, ΔSCF vs. $-E_{\mathrm{HOMO}}$, to understand the accuracy and intrinsic limitations of each theoretical approach. Among all of the theoretical methods studied here, we find that a non-empirically tuned range-separated approach (constructed to satisfy DFT-Koopmans' theorem for the anionic (N + 1)-electron system) provides the best accuracy for both metrics (ΔSCF and $-E_{\mathrm{HOMO}}$) as well as for both basis sets. In contrast, the electron affinities obtained from "converged" E_{HOMO} calculations with conventional XC functionals and smaller basis sets exhibit severe problems – the majority of these E_{HOMO} values are predicted to be positive, incorrectly implying that these anions are formally unbound. While the purely nonlocal HF method does give negative E_{HOMO} values and bound anions, there is a delicate balance between exchange and correlation, and the lack of electron correlation in HF yields errors that are nearly twice that of a non-empirically tuned range-separated approach (which correctly balances short range correlation with long-range exchange by satisfying DFT-Koopmans' theorem).

To address this conundrum of positive E_{HOMO} values, other researchers have suggested to compute the orbitals using HF (where E_{HOMO} is correctly predicted to be negative) but use the HF density to non-self-consistently evaluate the energy with an XC potential. While this procedure will formally result in a bound anion with a negative E_{HOMO},

the calculation of electronic properties, such as electronic couplings or gradients, becomes ill-defined since the potential is evaluated with one approach while the energy is non-self-consistently evaluated with another approximation. We instead propose the following alternative: use a non-empirically tuned procedure to satisfy DFT-Koopmans' theorem for the anionic (N+1) electron system, and use the resulting tuned XC functional to self-consistently evaluate both orbital energies and electron affinities. This procedure should yield correct E_{HOMO} values and well-defined electronic couplings/gradients since the potential (and, hence, the electronic energy) is obtained from the derivative of an energy functional. Finally, we examine the orbital energies and electron affinities in the context of the electronic energy, E, as a function of electronic number, N, including fractional numbers of electrons. We find that the non-empirically tuned LC-BLYP functional yields a nearly-exact straight line as a function of the fractional charge in the system, and plots of the deviation from linearity imply that the non-empirically tuned LC-BLYP is nearly SIE-free. Moreover, a deeper analysis of the E vs. N curves demonstrates that the non-empirically tuned LC-BLYP functional does not exhibit any tendency towards a flattening or fractional electron loss, resulting in anions that are accurately described and correctly bound for both basis sets. Taken together, these calculations and analyses provide a natural methodology for obtaining accurate and formally-correct bound anions with well-defined electronic properties (such as electronic gradients and couplings) in a fully self-consistent approach.

Chapter 2. Halogen Bonding Interactions: Revised Benchmarks and a New Assessment of Exchange vs. Dispersion

Abstract

We present a new analysis of exchange and dispersion effects for calculating halogen-bonding interactions in a wide variety of complex dimers (69 total) within the XB18 and XB51 benchmark sets. Contrary to previous work on these systems, we find that dispersion plays a more significant role than exact exchange in accurately calculating halogen-bonding interaction energies. In particular, we find that even if the amount of exact exchange is non-empirically tuned to satisfy known DFT constraints, we still observe an overall improvement in predicting dissociation energies when dispersion corrections are applied, in stark contrast to previous studies (*J. Chem. Theory Comput.* **2013**, *9*, 1918-1931). In addition to these new analyses, we correct several (14) inconsistencies in the XB51 set, which is widely used in the scientific literature for developing and benchmarking various DFT methods. Together, these new analyses and revised benchmarks emphasize the importance of dispersion and provide corrected reference values that are essential for developing/parameterizing new DFT functionals specifically for complex halogen-bonding interactions.

Introduction

Over the past decade, halogen bonding (XB) interactions have emerged as new bonding motifs that are now recognized to play a significant role in biochemistry,[68-69]

materials chemistry,[70-71], enzyme-substrate interactions, and polymer interactions.[72] The XB concept is analogous to conventional hydrogen bonding[73] (HB) in that a non-covalent bond forms between an electron donor and acceptor. On an electronic level, XB occurs when a halogen atom X acts as a Lewis acid (the XB donor) by accepting an electron from a neighboring atom (the XB acceptor). This bonding interaction is illustrated in Figure 6 for the specific case of $Br_2 \cdots$pyridine where the halogen atom X (i.e., Br) forms a halogen bond with a Lewis base, B (i.e., pyridine).

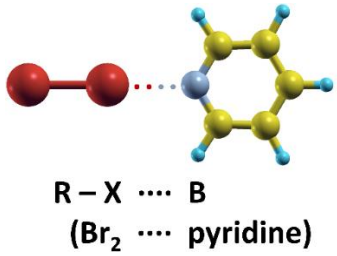

Figure 6. A prototypical halogen bond (XB) in which a halogen atom X (Br) forms a non-covalent bond with a Lewis base B (pyridine).

While halogen atoms often interact with electrophilic molecules due to the halogen's partial negative charge, bonds between halogens and negatively charged molecules can form as well. Both experimental and computational data[74-78] support these claims and show that halogens in close proximity to electrophiles (less than the sum of the atom's van der Waals radii) form bonds between 90°–120° relative to the R–X bond, whereas bonds form at angles close to 180° in nucleophiles. The latter interaction between halogens and nucleophilic molecules is considered halogen bonding.

The notion of halogens bonding to both types of molecules was initially puzzling since it implied that halogens could be treated as being either entirely positive or entirely

negative. This idea was heavily investigated by Politzer in 2008[79] and further justified in 2010,[80] where it was shown that this halogen/nucleophilic interaction occurs as a result of inductive effects of the attached R group. Depending on the size and net charge of R, the electron density can be pulled away from the attached halogen atom, and a small positive electrostatic potential is created directly across the R group on the outermost portion of the halogen's surface. This positive region is referred to as the σ-hole[81] and is the site of XB formation. Consequently, since the σ-hole is formed at a 180° angle with respect to the R group,[82] the interaction between nucleophiles and halogens is necessarily linear.

The strength of the XB depends not only on the electron-withdrawing power of the attached R group but also on the stability of the halogen atom. It has been observed[80, 82] that less electronegative halogens produce stronger halogen bonds: iodine forms stronger halogen bonds than bromine, bromine forms stronger halogen bonds than chlorine, and so forth. While it was once thought that only iodine, bromine, and chlorine were capable of forming halogen bonds, recent work has indicated that fluorine can participate in halogen bonding interactions as well, under special circumstances.[83]

Because of their unique bonding interactions, halogen bonding has attracted significant attention from theoretical and computational chemists to test the accuracy of various computational methods by decomposing XB contributions due to electrostatics, dispersion, polarization, and charge transfer.[80, 84] Recently, in 2013, Kozuch and Martin[85] carried out an extensive study of these contributions in two groups of dimers: 18 small dimers (the "XB18" benchmark set) and 51 larger dimers (the "XB51" set) with a broad range of dissociation energies. Based on their extensive benchmarks, the authors concluded

with the following statements: (1) "A high amount of exact exchange is necessary for good geometries and energies," and (2) "dispersion corrections tend to be detrimental, in spite of the fact that XB is considered a noncovalent interaction." In particular, we found the second statement on dispersion corrections to be particularly puzzling since, as previously mentioned, XB is a noncovalent interaction and should, therefore, be more accurately captured with dispersion corrections than without.

Motivated by these surprising findings, we re-assess the effects of exact exchange vs. dispersion on these halogen-bonding interactions using (1) both conventional range-separated and non-empirically tuned range-separated functionals and (2) a variety of dispersion corrections. While one can arbitrarily add a portion of exact exchange in any DFT functional, we use the non-empirical tuning procedure in this work to provide a rigorous way of incorporating exchange to both satisfy known DFT constraints and to contest previous claims that exact exchange plays a dominant role in halogen bond interactions.[85] In addition to these new calculations, we correct several, (i.e., 14) of the discrepancies in the widely-used XB51 benchmark set by providing revised benchmarks in this work. Finally, we give a detailed analysis of exact exchange vs. dispersion effects in halogen-bonding systems, and we discuss their relative importance in accurately calculating the complex interactions in these challenging systems.

Methodology

Figures 7 and 8 depict the various molecular dimers included in the XB18 and XB51 benchmark sets, respectively. The XB18 set was intentionally constructed by

Kozuch and Martin[85] to only contain halogen bonding interactions for small systems, allowing for highly accurate CCSD(T)/aVQZ geometry optimizations and single-point energies at the CCSD(T)/CBS level of theory. Specifically, this set contains all nine combinations of diatomic halogen donors (Br_2, BrI, ClBr, ClI, FBr, FI, HBr, HI, and I_2) with two halogen acceptors (NCH and H_2CO). As shown in Figure 7, all of the dimer geometries that include the cyanide molecule are linear, and all geometries with formaldehyde are planar.

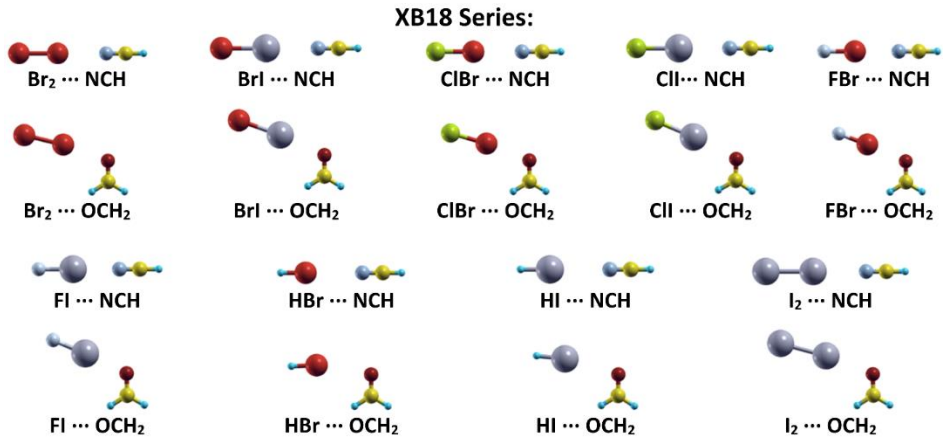

Figure 7. Molecular geometries in the XB18 benchmark set. This set contains all nine combinations of diatomic halogen donors (Br_2, BrI, ClBr, ClI, FBr, FI, HBr, HI, and I_2) with two halogen acceptors (NCH and H_2CO).

The XB51 set (also constructed by Kozuch and Martin[85]) is much broader than the XB18 set and consists of six series of 10 dimers in which three series vary the Lewis acid, and three vary the Lewis base (Figure 8). This more extensive benchmark set was designed to cover a broad distribution of dissociation energies ranging from the weak FCCH-based dimers to the strongly bonded organometallic systems that include $PdHP_2Cl$. Due to the larger sizes of the XB51 dimers, Kozuch and Martin carried out geometry optimizations at

the ωB97X/aVTZ level of theory with single-point energies computed using an MP2-based extrapolation of the CCSD(T) energy, denoted as $E_{\mathrm{CBS/MP2(Q5)}}^{\mathrm{CCSD(T)/aVTZ}}$ in their original paper. We critically test the contributions of exact exchange and dispersion in both of these sets (in addition to providing revised benchmark values for the XB51 set), as described in detail below.

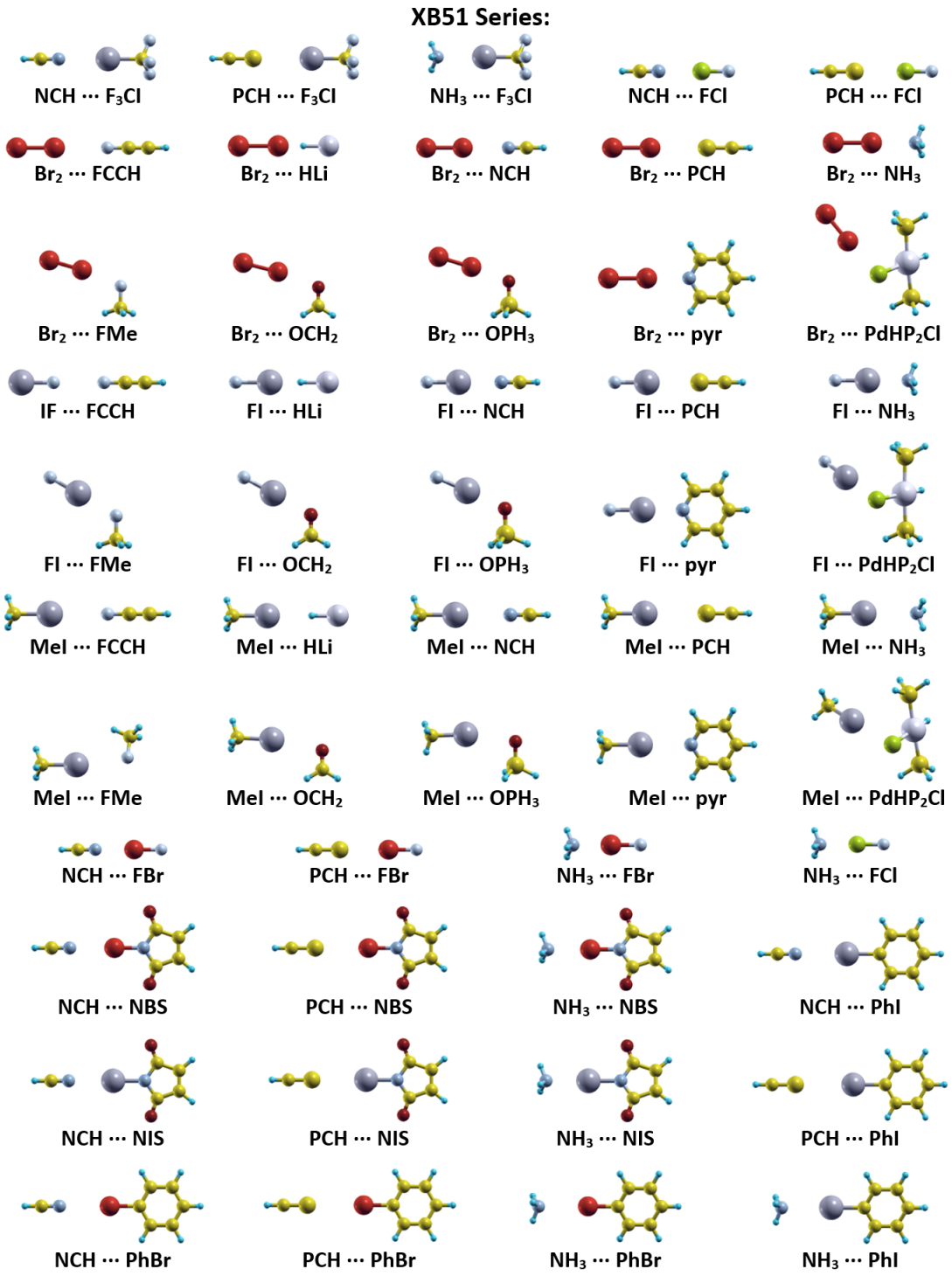

Figure 8. Molecular geometries in the XB51 benchmark set. This set covers a broad distribution of dissociation energies ranging from the weak FCCH-based dimers to the strongly bonded organometallic $PdHP_2Cl$-based dimers.

Contributions from Exact Exchange: Motivated by Kozuch and Martin's assessment that exact exchange may play the most important role in halogen bond formation,[85] we first focused on non-empirically tuning the contribution of exact exchange in a range-separated functional. While one can arbitrarily add a portion of exact exchange in any DFT functional, the non-empirical tuning procedure used here provides a rigorous way of incorporating exchange to both satisfy known DFT constraints (i.e. Koopman's theorem[86]) and to critically test previous claims that exact exchange plays a dominant role in halogen bond interactions. Throughout this entire study, all calculations were carried out with the long-range corrected ωPBE functional (LC-ωPBE), which is composed of (1) a short-range ωPBE approximation that satisfies the exchange-hole normalization condition for all values of ω and (2) a long-range portion of exact exchange that enforces a rigorously correct 100% contribution of asymptotic Hartree-Fock exchange, which we[46-50, 87] and others[51-52] have found to be essential for accurately describing long-range charge-transfer excitations, anions, orbital energies, and valence excitations.

In contrast to conventional hybrid functionals that use a constant fraction of Hartree-Fock exchange, range-separated functionals[88-89] mix short range density functional exchange with long-range Hartree-Fock exchange by partitioning the electron repulsion operator into short and long range terms (i.e., the mixing parameter is a function of electron coordinates). In its most general form, the partitioning of the interelectronic Coulomb operator is given by:[90-91]

$$\frac{1}{r_{12}} = \frac{1 - [\alpha + \beta \cdot \mathrm{erf}(\omega \cdot r_{12})]}{r_{12}} + \frac{\alpha + \beta \cdot \mathrm{erf}(\omega \cdot r_{12})}{r_{12}}. \qquad (4)$$

The "erf" term denotes the standard error function, r_{12} is the interelectronic distance between electrons 1 and 2, and ω is the range-separation parameter in units of Bohr^{-1}. The other parameters, α and β, satisfy the following constraints: $0 \leq \alpha + \beta \leq 1$, $0 \leq \alpha \leq 1$, and $0 \leq \beta \leq 1$. The α parameter allows for a contribution of Hartree-Fock exchange over the entire range by a factor of α, and the parameter β allows us to incorporate long-range asymptotic Hartree-Fock exchange by a factor of $\alpha + \beta$. Previous work by us[49] and others[92-93] has shown that maintaining a full 100% asymptotic contribution of HF exchange (i.e. fixing $\alpha + \beta = 1.0$) is essential for accurately describing electronic properties in even relatively simple molecular systems. However, the expression $\alpha + \beta = 1.0$ still contains one degree of freedom, and the choice of α will automatically fix the value of β. More recent work from us[61, 94] and others[95-98] has shown that some amount of short-range Hartree-Fock exchange (i.e., nonzero values for α) can lead to improved electronic properties and charge-transfer effects. Therefore, for the LC-ωPBE functional used in this work, we chose the fixed values of $\alpha = 0.2$ and $\beta = 0.8$ in conjunction with tuning the range-separation parameter ω via the non-empirical procedure by Baer and Kronik[55-57] discussed below. These particular values for α and β were chosen based on a recent study by Kronik et al.[97], which showed that (non-empirically tuned) values of $\alpha \sim 0.2$ (i.e., 20% short-range Hartree-Fock exchange) in conjunction with long-range exchange were able to accurately predict the electronic properties of various chemical systems.

As stated above, the range-separation parameter ω can be non-empirically tuned by satisfying Koopman's theorem,[86] which ensures the equality of the ionization potential (IP) and the negative of the highest occupied molecular orbital (HOMO) energy for an *N*-

electron system. The individual IP(N) values are found by taking the difference in ground state energies (ΔSCF) between the N and $N-1$ electron systems. Self-consistently tuning ω with this procedure is theoretically justified by the fact that the exact exchange-correlation functional would automatically satisfy this condition. Although several numerical schemes exist, a range-separation parameter, ω, that approximately satisfies this condition can be obtained by minimization of the following function for each molecular system:

$$J^2(\omega) = [\varepsilon^{\omega}_{\mathrm{HOMO}}(N) + \mathrm{IP}^{\omega}(N)]^2 + [\varepsilon^{\omega}_{\mathrm{HOMO}}(N+1) + \mathrm{IP}^{\omega}(N+1)]^2, \qquad (5)$$

In the expression above, both $\varepsilon^{\omega}_{\mathrm{HOMO}}(N)$ and $\mathrm{IP}^{\omega}(N)$ are calculated with the same value of the range-separation parameter, ω. The $N+1$ energies in the second term of Eq. 5 are included as a way of indirectly tuning the HOMO and LUMO energies of the *N*-electron system, since a formal equivalent of Koopman's theorem does not exist that relates the LUMO energy to the electron affinity. All $\varepsilon^{\omega}_{\mathrm{HOMO}}$ and IP^{ω} values in this work were calculated for each dimer with the LC-ωPBE$_{\alpha=0.2,\beta=0.8}$ functional. In order to determine the optimal range-separation value for each halogen-bonding dimer, we carried out several single-point energy calculations by varying ω from 0.05 to 0.7 (in increments of 0.05) for each of the N, $N+1$, and $N-1$ electron states. Spline interpolation was used to refine the minimum of each curve, providing the optimal ω for each halogen-bonding dimer. With the optimal ω determined for each dimer, the dissociation energy was calculated with the following expression.

$$E_{\mathrm{dissociation}}(\omega) = E_{\mathrm{monomer1}}(\omega) + E_{\mathrm{monomer2}}(\omega) - E_{\mathrm{dimer}}(\omega). \qquad (6)$$

It is important to note in Eq. (6) that $E_{\mathrm{monomer1}}(\omega)$, $E_{\mathrm{monomer2}}(\omega)$, and $E_{\mathrm{dimer}}(\omega)$ are all calculated with the same value of the range-separation parameter which we always take to be the optimal ω value for the dimer. We choose the dimer as a suitable reference point for determining ω for all three chemical species in Eq. (6) due to size-consistency issues inherent to the non-empirical tuning procedure.[99]

Finally, to provide a systematic comparison to Kozuch and Martin's prior work,[85] we used the same basis sets (aVQZ for XB18 and a counterpoise-corrected aVTZ+CP basis set for XB51) used in their previous work. It should also be mentioned that Kozuch and Martin only incorporated BSSE and counterpoise corrections in the XB51 set (and not the XB18 set), and to ensure a direct comparison to their prior work, we also only included counterpoise corrections in the XB51 set.

Contributions from Dispersion: To assess the importance of dispersion corrections in halogen-bonding interactions, we assessed two different types of "D3" dispersion corrections[100] that were used in the original work by Kozuch and Martin.[85] Conventional DFT methods lack long-range dispersion forces, and Grimme's D3 approach adds an atomic pairwise dispersion correction to the Kohn-Sham portion of the total energy ($E_{\mathrm{KS-DFT}}$) as

$$E_{\mathrm{DFT-D3}} = E_{\mathrm{KS-DFT}} + E_{\mathrm{disp}}, \tag{7}$$

where E_{disp} is given by

$$E_{\mathrm{disp}} = -\sum_{i=1}^{N_{\mathrm{at}}-1}\sum_{j=i+1}^{N_{\mathrm{at}}} f_{\mathrm{d},6}(R_{ij})\frac{C_{6,ij}}{R_{ij}^{6}} + f_{\mathrm{d},8}(R_{ij})\frac{C_{8,ij}}{R_{ij}^{8}}, \tag{8}$$

and the summation is over all atom pairs i and j, with R_{ij} denoting their interatomic distance. The $C_{6,ij}$ and $C_{6,ij}$ parameters are sixth- and eighth-order dispersion coefficients that are geometry dependent and are adjusted as a function of the local geometry around atoms i and j. In order to avoid near-singularities for small interatomic distances, $f_{\mathrm{d},6}$ and $f_{\mathrm{d},8}$ are damping functions for the additional R_{ij}^{-6} and R_{ij}^{-8} repulsive potentials, respectively. In the original DFT-D3Zero method, the $f_{\mathrm{d},6}$ and $f_{\mathrm{d},8}$ damping functions (and thus E_{disp}) were constructed to approach zero when $R_{ij} = 0$. A critical disadvantage of this zero-damping approach is that at small and medium distances, the atoms experience repulsive forces leading to even longer interatomic distances than those obtained without dispersion corrections.[101] As a practical solution for this counter-intuitive observation, Becke and Johnson[102-104] proposed the DFT-D3BJ method which contains modified expressions for $f_{\mathrm{d},6}$ and $f_{\mathrm{d},8}$ that lead to a constant contribution of E_{disp} to the total energy when $R_{ij} = 0$. We assess the performance of both the D3Zero and D3BJ dispersion corrections by adding them to the standard LC-ωPBE$_{\alpha=0,\beta=1.0}$(ω = 0.47) functional (abbreviated simply as LC-ωPBE throughout the rest of this work) and to our non-empirically tuned LC-ωPBE$_{\alpha=0.2,\beta=0.8}$ approach for all of the halogen-binding dimers in this work. It is worth mentioning that the D3 dispersion correction is a post-SCF add-on to the Kohn-Sham total energy via Eq. 7 and, therefore, the D3 correction does not alter the $\varepsilon_{\mathrm{HOMO}}^{\omega}$ or IP$^{\omega}$ energies in the expression for $J^2(\omega)$ in Eq. 5. As such, the non-empirical tuning approach is numerically independent from the D3 dispersion correction, allowing us to simply add both of these contributions together to obtain the resulting halogen-bonding interaction energies.

To make a consistent comparison with the previous study by Kozuch and Martin, identical molecular geometries obtained from Ref. [85] were used throughout this work. Similaraly, all of our dissociation energies were compared to their reference benchmark values obtained with CCSD(T)/CBS for XB18 dimers and CCSD(T)/CBS-MP2(Q5) for XB51 dimers to quantify the relative errors for each method. All DFT calculations were carried out with the Gaussian 09 package[105] using default SCF convergence criteria (density matrix converged to at least 10^{-8}) and the default DFT integration grid (75 radial and 302 angular quadrature points). The additional D3 dispersion corrections (D3Zero and D3BJ) were calculated by adding these to the DFT total energies using the DFT-D3 program by Grimme et al.[106] For future reference and reproducibility, all of our ground state energies and dissociation energies can be found in the Supporting Information.

Results and Discussion

It is extremely important to mention that during the compilation and analysis of our results, we noticed several discrepancies in the reference dissociation energies provided by Kozuch and Martin for the XB51 series. Specifically, the reference energies listed in their Supporting Information are not consistent with those listed in Table 5 within the main text of their work,[85] giving different theoretical values for 14 of these dimers. In addition, there are also internal inconsistencies within the same table that define two (significantly) different reference dissociation energies for the dimers $Br_2\cdots NCH$, $Br_2\cdots NH_3$, $FI\cdots NCH$, and $FI\cdots NH_3$. We were able to determine the correct reference energies by comparing the values provided in their main text to the CCSD(T)/AVTZ + DF-MP2(Q5) values in their

Supporting Information (Figure SI-1 in our Supporting Information gives a detailed, color-coded comparison of these inconsistencies). To bring closure and correct the scientific literature on these important benchmark values, we provide the corrected values in Table 4, and it is these dissociation energy values that we use as our reference for comparison.

Table 4. Revised benchmark dissociation energies (in kcal/mol) for the XB51 set, at the $E_{\mathrm{CBS/MP2(Q5)}}^{\mathrm{CCSD(T)/aVTZ}}$ level of theory. Energies shown in bold are values that have been corrected from ref. [85].

	X acc.				X donor		
X donor	PCH	NCH	NH_3	X acc.	MeI	BrBr	FI
PhBr	0.85	1.15	2.02	FCCH	0.50	0.74	0.29
MeI	0.85	1.42	2.73	PCH	0.85	1.18	2.74
PhI	0.92	1.87	3.33	NCH	1.42	**3.61**	**9.33**
F_3CI	0.89	3.61	5.88	FMe	1.70	**2.87**	**5.97**
Br_2	1.18	3.61	7.29	OCH_2	2.39	4.41	9.94
NBS	1.19	4.32	8.02	NH_3	2.73	**7.29**	**17.11**
FCl	1.16	4.81	10.54	OPH_3	3.34	**5.95**	**13.36**
NIS	1.53	5.91	10.99	Pyr	3.61	**9.07**	**20.34**
FBr	2.07	7.53	15.30	HLi	3.62	**23.11**	**33.79**
FI	2.74	9.33	17.11	$PdHP_2Cl$	5.05	**9.00**	**17.66**

With these corrected benchmark values in hand, we first discuss the effect of incorporating exact exchange on the halogen-bonding interactions for the XB18 and XB51 benchmark sets. Figure 9 shows the smooth curves that result from computing J^2 as a function of ω for a representative set of halogen-bonding dimers. The optimally tuned ω values for all of the halogen-bonding dimers are summarized in Table 5. To create succinct

figures and graphs similar to the ones in Kozuch and Martin's study, we split the XB51 series into two groups: the first group contains dimers with the halogen acceptors PCH, NCH, and NH_3, (each with the same set of donors) and the second group contains dimers with the halogen donors MeI, Br_2, and FI (each with the same set of acceptors).

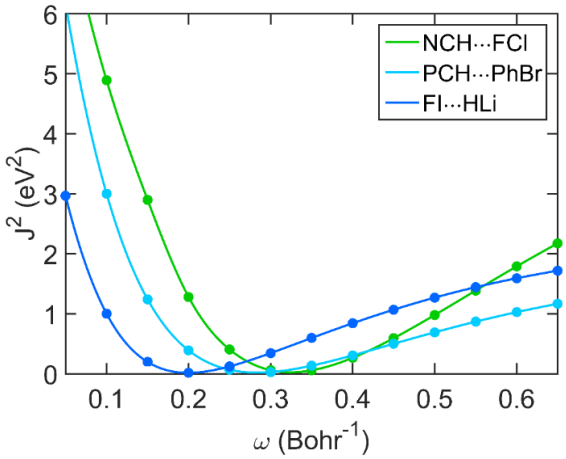

Figure 9. Plots of J^2 (Eq. 2) as a function of ω for a representative set of halogen bonding dimers.

Table 5: Optimal ω values for each halogen-bonding dimer in units of $bohr^{-1}$.

XB18 Dimers		XB51 Dimers			
	Opt ω		Opt ω		Opt ω
$Br_2\cdots NCH$	0.283	$NCH\cdots F_3CI$	0.257	$Br_2\cdots FCCH$	0.297
$Br_2\cdots OCH_2$	0.279	$NCH\cdots FBr$	0.297	$Br_2\cdots FMe$	0.292
$BrI\cdots NCH$	0.304	$NCH\cdots FCl$	0.324	$Br_2\cdots HLi$	0.202
$BrI\cdots OCH_2$	0.232	$NCH\cdots NBS$	0.221	$Br_2\cdots NCH$	0.284
$ClBr\cdots NCH$	0.288	$NCH\cdots NIS$	0.217	$Br_2\cdots NH_3$	0.267
$ClBr\cdots OCH_2$	0.284	$NCH\cdots PhBr$	0.206	$Br_2\cdots OCH_2$	0.281
$ClI\cdots NCH$	0.259	$NCH\cdots PhI$	0.201	$Br_2\cdots OPH_3$	0.269
$ClI\cdots OCH_2$	0.239	$NH_3\cdots F_3CI$	0.254	$Br_2\cdots PCH$	0.266
$FBr\cdots NCH$	0.295	$NH_3\cdots FBr$	0.295	$Br_2\cdots PdHP_2Cl$	0.176
$FBr\cdots OCH_2$	0.294	$NH_3\cdots FCl$	0.299	$Br_2\cdots pyr$	0.237
$FI\cdots NCH$	0.269	$NH_3\cdots NBS$	0.214	$FI\cdots FCCH$	0.304
$FI\cdots OCH_2$	0.257	$NH_3\cdots NIS$	0.212	$FI\cdots FMe$	0.288
$HBr\cdots NCH$	0.332	$NH_3\cdots PhBr$	0.205	$FI\cdots HLi$	0.262
$HBr\cdots OCH_2$	0.296	$NH_3\cdots PhI$	0.199	$FI\cdots NCH$	0.271
$HI\cdots NCH$	0.299	$PCH\cdots F_3CI$	0.258	$FI\cdots NH_3$	0.278
$HI\cdots OCH_2$	0.282	$PCH\cdots FBr$	0.259	$FI\cdots OCH_2$	0.258
$I_2\cdots NCH$	0.250	$PCH\cdots FCl$	0.279	$FI\cdots OPH_3$	0.264
$I_2\cdots OCH_2$	0.223	$PCH\cdots NBS$	0.218	$FI\cdots PCH$	0.260
		$PCH\cdots NIS$	0.212	$FI\cdots PdHP_2Cl$	0.222
		$PCH\cdots PhBr$	0.187	$FI\cdots pyr$	0.218
		$PCH\cdots PhI$	0.205	$MeI\cdots FCCH$	0.267
				$MeI\cdots FMe$	0.267
				$MeI\cdots HLi$	0.442
				$MeI\cdots NCH$	0.266
				$MeI\cdots NH_3$	0.264
				$MeI\cdots OCH_2$	0.262
				$MeI\cdots OPH_3$	0.257
				$MeI\cdots PCH$	0.251
				$MeI\cdots PdHP_2Cl$	0.219
				$MeI\cdots pyr$	0.229

Contributions from Exact Exchange: As previously mentioned, Kozuch and Martin stated that "a high amount of exact exchange is necessary for good geometries and energies."[85] To critically test this claim, we compared their PBE (no Hartree-Fock exchange) and "default" LC-ωPBE (ω fixed at 0.47) benchmarks to dissociation energies obtained from our non-empirically tuned LC-ωPBE$_{\alpha=0.2,\beta=0.8}$ functional. Figure 10 gives a visual comparison of the absolute errors in the dissociation energy, and Table 6 summarizes the mean absolute errors (MAEs) and mean signed errors (MSEs) for each of the DFT methods. Taken together, both Figure 10 and Table 6 show an overall degradation in the accuracy of LC-ωPBE compared to PBE (the MAE increases from 1.14 to 1.35 kcal/mol), suggesting that an un-tuned (ω = 0.47) amount of exchange actually worsens the dissociation energies for these XB dimers. However, when we applied the non-empirical tuning procedure to the LC-ωPBE$_{\alpha=0.2,\beta=0.8}$ functional (which, again, satisfies known DFT constraints), we found that the MAEs were not significantly better than PBE (see Table 6). For the smaller dimers in the XB18 series, the absolute error in the dissociation energies actually increased for FBr···NCH and FI···NCH compared to the untuned LC-ωPBE functional (although these energies were still more accurate than the values obtained with the bare PBE functional). Nevertheless, we observed more severe problems with the following XB51 dimers: NH_3···FBr, FI···FCCH, FI···HLi, FI···NCH, FI···NH_3, and FI···OPH_3 all exhibited dissociation energies that were all worsened by the tuning process. We attribute these errors to the high electronegativity of fluorine in these small molecules, which has been known to be problematic in prior computational studies for accurately calculating XB interactions.[81-83] As a whole, these results demonstrate that

the inclusion of exact exchange–even with a non-empirically tuned amount of exchange–only has a marginal effect on improving the accuracy in computing halogen-bonding interactions, in contrast to previous studies.[85]

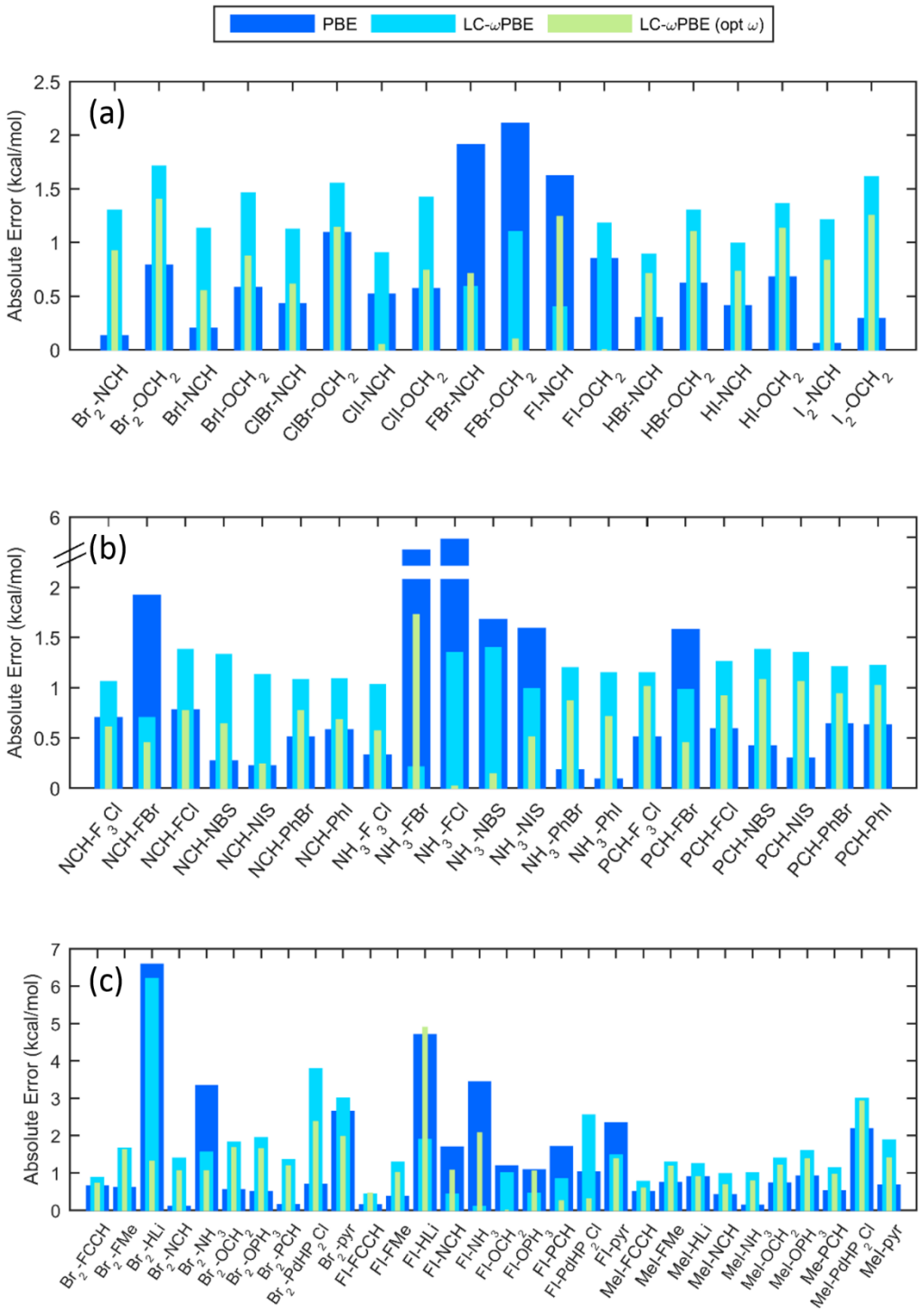

Figure 10. Absolute errors in the dissociation energy predicted by various DFT functionals without dispersion for halogen-bonding dimers within the (a) XB18 and (b and c) XB51 benchmark sets.

Table 6. Mean absolute errors in kcal/mol for halogen-bonding dissociation energies obtained with various DFT methods.

	PBE[a]	LC-ωPBE[b]	LC- ωPBE (opt ω)	LC-ωPBE + D3BJ[b]	LC-ωPBE + D3BJ (opt ω)	LC-ωPBE + D3Zero	LC-ωPBE + D3Zero (opt ω)
XB18	0.73	1.18	0.78	0.30	0.57	0.38	0.40
XB51	1.28	1.41	1.06	0.65	0.99	0.57	0.75
Overall	1.14	1.35	0.99	0.56	0.88	0.52	0.66

[a] Based on benchmarks from Ref. [85]

[b] Based on the default range-separation value of $\omega = 0.47$ used in Ref. [85]

Contributions from Dispersion: We next investigated the effects of adding two different types of dispersion corrections based on Kozuch and Martin's assertion that "dispersion corrections tend to be detrimental" for accurately calculating XB dissociation energies.[85] Figure 11 gives a visual comparison of the absolute errors, and Table 6 summarizes the MAEs and MSEs for each of the DFT methods. In general, adding either the D3BJ or D3Zero corrections to the standard LC-ωPBE functional significantly improved the overall accuracy, in contrast to Kozuch and Martin's assessment that dispersion corrections worsen XB dissociation energies. Specifically, the final MAEs for the XB51 set are nearly three times lower for each D3 method compared to the parent LC-ωPBE functional. While the D3Zero correction performed slightly better than D3BJ, the total difference between the two methods is negligible. It is interesting to note that both dispersion corrections give even lower MAEs for smaller dimers in the XB18 set, with errors that are almost four times lower than the standard LC-ωPBE functional. In the XB18 series, the FI···NCH dimer was the only exception in which the D3BJ correction increased the absolute error. For the XB51 series, two dimers were more accurate before the inclusion of either dispersion corrections (NH_3···FBr and FI···NH_3). In addition, there were a few

cases where D3Zero improved results whereas the D3BJ correction worsened them (NCH···NIS, FI···NCH, and FI···OPH_3) and only one case where D3BJ improved whereas D3Zero worsened them (FI···FCCH). Regardless of these few exceptions, we observed a clear overall improvement in predicting dissociation energies when the D3BJ or D3Zero corrections are applied to the standard LC-ωPBE functional (regardless if the exchange was non-empirically tuned or not), which is in stark contrast to previous studies.[85]

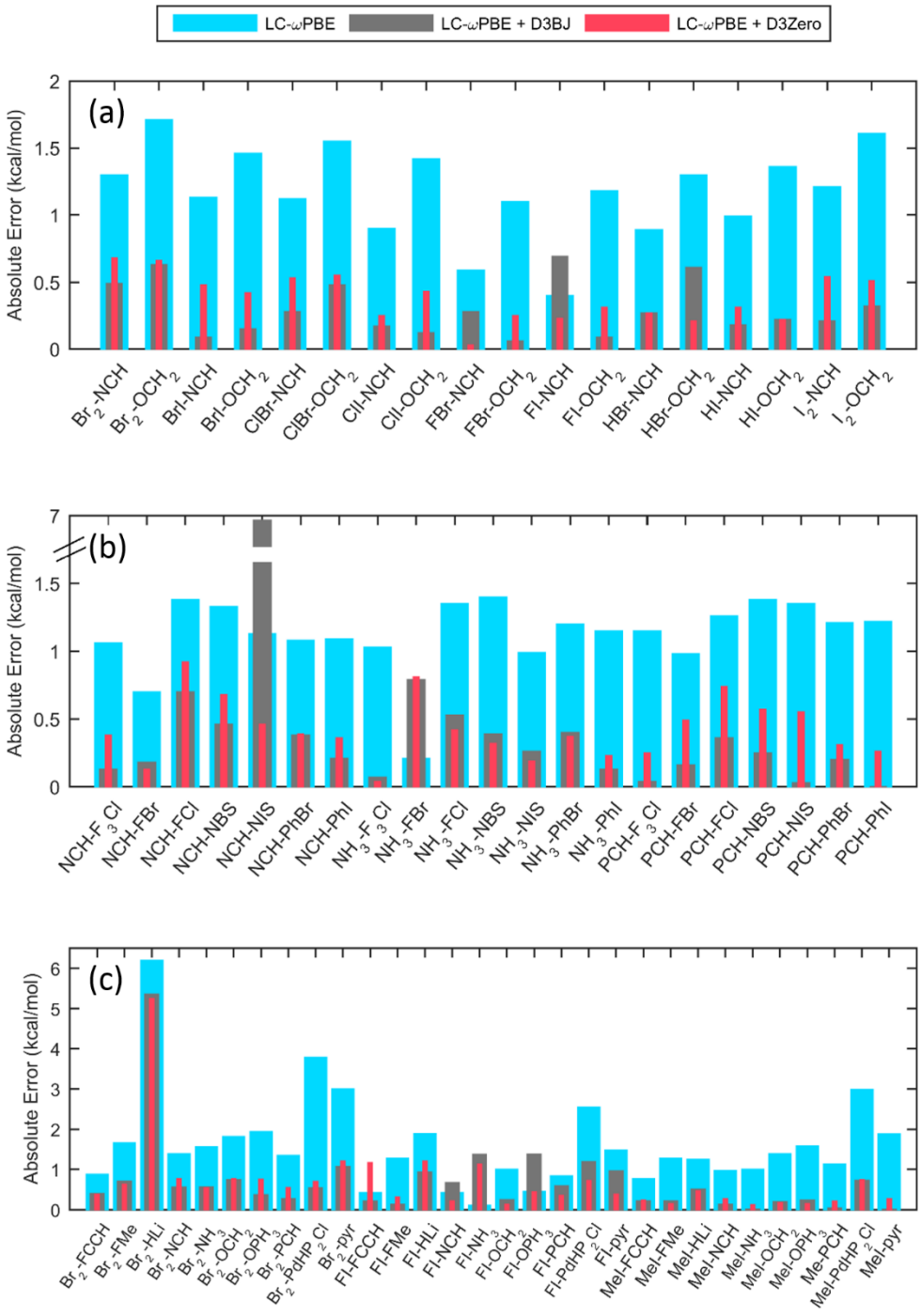

Figure 11. Absolute errors in the dissociation energy predicted by the standard LC-ωPBE functional (ω = 0.47), with and without dispersion for halogen-bonding dimers within the (a) XB18 and (b and c) XB51 benchmark sets.

It is interesting to note that the error analysis becomes slightly more complicated when dispersion corrections are added to the non-empirically tuned LC-ωPBE$_{\alpha=0.2,\beta=0.8}$ functional (see Figure SI-2 in the Supporting Information). For approximately one-third of the dimers, we incur larger errors when dispersion corrections are added to the non-empirically tuned LC-ωPBE$_{\alpha=0.2,\beta=0.8}$ functional, regardless of the type of D3 correction used. More interestingly, we also noticed from Figure SI-2 that nearly every dimer whose accuracy was worsened with dispersion involved a fluorine-containing halide, which again corroborates previous studies that found fluorine to be problematic for accurately calculating XB interactions.[81-83] We have summarized the mean signed error (MSE), root mean square deviation (RMSD), and maximum error for each method in Figure 12 and Table 7. Taken together, both Figure 12 and Table 7 clearly indicate that adding the D3BJ or D3Zero corrections to the standard LC-ωPBE functional gives the lowest overall MSE and RMSD values (with LC-ωPBE+D3BJ boasting a nearly zero MSE). We also note that both the LC-ωPBE+D3Zero and LC-ωPBE+D3BJ functionals gave significantly lower MSE and RMSD values than their non-empirically tuned counterparts, indicating that non-empirically tuned exchange actually worsens XB interaction energies. Collectively, Figures 10-12 and the MSE errors summarized in Table 7 indicate that dispersion corrections play a much larger role than exact exchange in capturing halogen-bonding interactions (regardless if the exchange is non-empirically tuned or not).

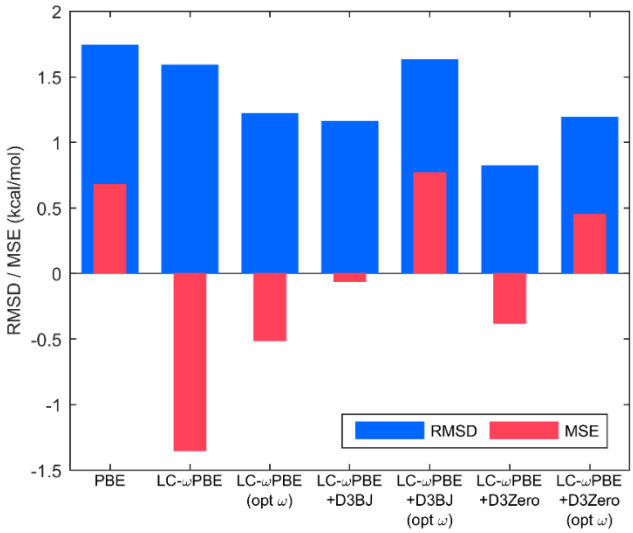

Figure 12. Root mean square deviation (RMSD) and mean signed error (MSE) for halogen-bonding dissociation energies obtained with various DFT methods.

Table 7. Mean signed error (MSE), root-mean-square deviation (RMSD), and maximum error for halogen-bonding dissociation energies obtained with various DFT methods.

	XB18 Series			XB51 Series			Overall		
	MSE	RMSD	Max Error	MSE	RMSD	Max Error	MSE	RMSD	Max Error
PBE[a]	0.50	0.93	2.11	0.75	1.95	6.58	0.68	1.74	6.58
LC-ωPBE[a]	-1.18	1.30	-1.71	-1.41	1.70	-6.20	-1.35	1.59	-6.20
LC-ωPBE (opt ω)	-0.57	0.92	-1.40	-0.50	1.32	4.89	-0.51	1.22	4.89
LC-ωPBE + D3BJ	-0.16	0.35	0.69	-0.03	1.34	6.88	-0.06	1.16	6.88
LC-ωPBE + D3BJ (opt ω)	0.45	0.39	2.33	0.88	1.83	7.78	0.77	1.63	7.78
LC-ωPBE + D3Zero	-0.36	0.46	-0.68	-0.39	0.92	-5.24	-0.38	0.82	-5.24
LC-ωPBE + D3Zero (opt ω)	0.26	0.23	1.88	0.52	1.33	5.57	0.45	1.19	5.57

[a] Based on benchmarks from Ref. [85]

Conclusions

In this extensive study, we have revisited and analyzed several halogen-bonding interactions in a wide variety of complex dimers within the XB18 and XB51 set. To critically assess the effects of exact exchange and dispersion on these complex halogen-bonding interactions, we calculated new dissociation energies using both conventional range-separated and non-empirically tuned range-separated functionals in conjunction with a variety of dispersion corrections. These new calculations extend previous benchmark calculations on these systems as well as shed critical insight on the relative importance of exact exchange vs. dispersion in accurately calculating these interactions.

Contrary to previous studies on these systems, our analyses and results suggest that dispersion plays a more significant role than exact exchange in accurately calculating halogen-bonding interactions. While our numerical benchmarks verify the importance of dispersion in these systems, our analysis is also chemically intuitive – halogen-bonding effects are noncovalent interactions and should, therefore, be more accurately captured with dispersion corrections than without. Ultimately (and probably most importantly), we correct several (14) of the inconsistencies in the XB51 benchmark set by providing revised benchmarks in this work. A reference search in the Thomson Reuters Web of Science[107] shows that the original XB51 benchmarks have already been cited over 120 times, and the present study brings closure and corrects the scientific literature on these important benchmark values. In terms of DFT functional development for specifically improving halogen-bonding interactions, our analysis suggests that more emphasis should be placed

on improving dispersion effects rather than exact exchange, in contrast to prior studies on these systems.

Overall Conclusions

Throughout the first chapter of this thesis, we assessed the accuracy of orbital energies and electron affinities for the first three rows of elements on the periodic table (H-AR) by implementing multiple theoretical approaches in combination with standard and customized basis sets. During these calculations, electron affinities were found for these anions with the ΔSCF procedure and were then compared to the negative E_{HOMO} values. This is justified by Koopman's theorem for the anion and is meant to give a deeper insight to the limiting factors within each theoretical method. In summary, the nonempirically tuned range-separated method provides the best accuracy in both cases for the standard and the customized basis sets. While the HF method obtains negative E_{HOMO} values for the anions, suggesting that the atoms remain bound throughout the calculation, there exists a fine balance between the exchange and correlation potentials and the lack of electron correlation in HF produces errors that are almost twice as large as the nonempirically tuned range-separated method.

Also in Chapter 1, we found that the nonempirically tuned LC-BLYP functional yields nearly a straight line when comparing the electronic energies, E, as a function of electronic number, N, while the other cases deviate from linearity when including fractional numbers of electrons. This further suggests that the LC-BLYP functional results in an accurate description of bound anions, even with the smaller basis set, and provides a natural and self-consistent approach to defining accurate electronic properties of anions.

When applying the standard and nonempirically tuned long-range corrected methodology to halogen bonding dimers in Chapter 2, we saw that including exact

exchange was less effective at providing accurate dissociation energies. Additionally, our results suggest that one can obtain more accurate results when including dispersion corrections like D3Zero and D3BJ as opposed to solely relying on the effects of exact exchange to improve the results. We were also able to correct several inconsistencies that were provided in the original XB51 benchmark set, as noted and referenced in Chapter 2, and we show that a greater emphasis should be placed on improving dispersion effects instead of exact exchange when it comes to studying halogen-bonding interactions.

References

1. Engel, E.; Dreizler, R. M., Introduction. In *Density Functional Theory: An Advanced Course*, Springer Berlin Heidelberg: Berlin, Heidelberg, 2011; pp 1-9.

2. Koch, W. a. H., M. C., *A Chemist's Guide to Density Functional Theory*, Second ed., 2001.

3. Hohenberg, P. K., W., Inhomogenous Electron Gas. *Physical Review* **1964**, *136*, B864.

4. Kohn, W. S., L. J., Self-Consistent Equations Including Exchange and Correlation Effects. *Physical Review* **1965**, *140*, A1133.

5. Parr, R. G. Y., W., *Density-Functional Theory of Atoms and Molecules*; Oxford University Press: New York, 1989.

6. Watson, J. K. G., Effects of a Core Electric Dipole Moment on Rydberg States. *Mol Phys* **1994**, *81*, 277-289.

7. Kay, J. J.; Coy, S. L.; Petrović, V. S.; Wong, B. M.; Field, R. W., Separation of Long-Range and Short-Range Interactions in Rydberg States of Diatomic Molecules. *The Journal of Chemical Physics* **2008**, *128*, 194301.

8. Coy, S. L.; Grimes, D. D.; Zhou, Y.; Field, R. W.; Wong, B. M., Electric Potential Invariants and Ions-in-Molecules Effective Potentials for Molecular Rydberg States. *The Journal of Chemical Physics* **2016**, *145*, 234301.

9. Mitroy, J.; Safronova, M. S.; Charles, W. C., Theory and Applications of Atomic and Ionic Polarizabilities. *J. Phys. B: At., Mol. Opt. Phys.* **2010**, *43*, 202001.

10. Marante, C.; Argenti, L.; Martín, F., Hybrid Gaussian–***B***-Spline Basis for the Electronic Continuum: Photoionization of Atomic Hydrogen. *Physical Review A* **2014**, *90*, 012506.

11. Lopata, K.; Govind, N., Near and above Ionization Electronic Excitations with Non-Hermitian Real-Time Time-Dependent Density Functional Theory. *J Chem Theory Comput* **2013**, *9*, 4939-4946.

12. Sommerfeld, T.; Ehara, M., Complex Absorbing Potentials with Voronoi Isosurfaces Wrapping Perfectly around Molecules. *J Chem Theory Comput* **2015**, *11*, 4627-4633.

13. Verlet, J. R. R.; Bragg, A. E.; Kammrath, A.; Cheshnovsky, O.; Neumark, D. M., Observation of Large Water-Cluster Anions with Surface-Bound Excess Electrons. *Science* **2005**, *307*, 93-96.

14. Siefermann, K. R.; Liu, Y.; Lugovoy, E.; Link, O.; Faubel, M.; Buck, U.; Winter, B.; Abel, B., Binding Energies, Lifetimes and Implications of Bulk and Interface Solvated Electrons in Water. *Nat Chem* **2010**, *2*, 274-279.

15. Tang, Y.; Shen, H.; Sekiguchi, K.; Kurahashi, N.; Mizuno, T.; Suzuki, Y.-I.; Suzuki, T., Direct Measurement of Vertical Binding Energy of a Hydrated Electron. *Phys Chem Chem Phys* **2010**, *12*, 3653-3655.

16. Taylor, T. R.; Asmis, K. R.; Xu, C.; Neumark, D. M., Evolution of Electronic Structure as a Function of Size in Gallium Phosphide Semiconductor Clusters. *Chem Phys Lett* **1998**, *297*, 133-140.

17. Bundhun, A.; Abdallah, H. H.; Ramasami, P.; Schaefer, H. F., Germylenes: Structures, Electron Affinities, and Singlet−Triplet Gaps of the Conventional Xgecy3 (X = H, F, Cl, Br, and I; Y = F and Cl) Species and the Unexpected Cyclic Xgecy3 (Y = Br and I) Systems. *The Journal of Physical Chemistry A* **2010**, *114*, 13198-13212.

18. Chang, A. H. H.; Ermler, W. C.; Pitzer, R. M., Carbon Molecule (C60) and Its Ions: Electronic Structure, Ionization Potentials, and Excitation Energies. *The Journal of Physical Chemistry* **1991**, *95*, 9288-9291.

19. Dreuw, A.; Cederbaum, L. S., Multiply Charged Anions in the Gas Phase. *Chem Rev* **2002**, *102*, 181-200.

20. Han, H.; Zimmt, M. B., Solvent-Mediated Electron Transfer: Correlation between Coupling Magnitude and Solvent Vertical Electron Affinity. *J Am Chem Soc* **1998**, *120*, 8001-8002.

21. Kim, J. Y.; Lee, K.; Coates, N. E.; Moses, D.; Nguyen, T.-Q.; Dante, M.; Heeger, A. J., Efficient Tandem Polymer Solar Cells Fabricated by All-Solution Processing. *Science* **2007**, *317*, 222-225.

22. Shoaee, S.; Clarke, T. M.; Huang, C.; Barlow, S.; Marder, S. R.; Heeney, M.; McCulloch, I.; Durrant, J. R., Acceptor Energy Level Control of Charge Photogeneration in Organic Donor/Acceptor Blends. *J Am Chem Soc* **2010**, *132*, 12919-12926.

23. Rienstra-Kiracofe, J. C.; Tschumper, G. S.; Schaefer, H. F.; Nandi, S.; Ellison, G. B., Atomic and Molecular Electron Affinities: Photoelectron Experiments and Theoretical Computations. *Chem Rev* **2002**, *102*, 231-282.

24. Shore, H. B.; Rose, J. H.; Zaremba, E., Failure of the Local Exchange Approximation in the Evaluation of the ${\Mathrm{H}}^{-}$ Ground State. *Phys Rev B* **1977**, *15*, 2858-2861.

25. Schwarz, K., Instability of Stable Negative Ions in the Xα Method or Other Local Density Functional Schemes. *Chem Phys Lett* **1978**, *57*, 605-607.

26. Sen, K. D., Instability of Stable Negative Ions in Xα Method. *Chem Phys Lett* **1980**, *74*, 201-202.

27. Cole, L. A.; Perdew, J. P., Calculated Electron Affinities of the Elements. *Physical Review A* **1982**, *25*, 1265-1271.

28. Vydrov, O. A.; Scuseria, G. E., Ionization Potentials and Electron Affinities in the Perdew–Zunger Self-Interaction Corrected Density-Functional Theory. *The Journal of Chemical Physics* **2005**, *122*, 184107.

29. Jarcki, A. A.; Davidson, E. R., Density Functional Theory Calculations for F^-. *Chem Phys Lett* **1999**, *300*, 44-52.

30. van Leeuwen, R.; Baerends, E. J., Exchange-Correlation Potential with Correct Asymptotic Behavior. *Physical Review A* **1994**, *49*, 2421-2431.

31. Galbraith, J. M.; III, H. F. S., Concerning the Applicability of Density Functional Methods to Atomic and Molecular Negative Ions. *The Journal of Chemical Physics* **1996**, *105*, 862-864.

32. Lee, D.; Furche, F.; Burke, K., Accuracy of Electron Affinities of Atoms in Approximate Density Functional Theory. *The Journal of Physical Chemistry Letters* **2010**, *1*, 2124-2129.

33. Jensen, F., Describing Anions by Density Functional Theory: Fractional Electron Affinity. *J Chem Theory Comput* **2010**, *6*, 2726-2735.

34. Chattaraj, P. K.; Duley, S., Electron Affinity, Electronegativity, and Electrophilicity of Atoms and Ions. *Journal of Chemical & Engineering Data* **2010**, *55*, 1882-1886.

35. Gong, L.; Wu, X.; Li, W.; Qi, C.; Xiong, J.; Guo, W., Structures and Electron Affinities of Bro2f2 and Bro2f3. *Mol Phys* **2009**, *107*, 701-709.

36. Feng, X.; Li, Q.; Gu, J.; Cotton, F. A.; Xie, Y.; Schaefer, H. F., Perfluorinated Polycyclic Aromatic Hydrocarbons: Anthracene, Phenanthrene, Pyrene, Tetracene, Chrysene, and Triphenylene. *The Journal of Physical Chemistry A* **2009**, *113*, 887-894.

37. Bozkaya, U., The Extended Koopmans' Theorem for Orbital-Optimized Methods: Accurate Computation of Ionization Potentials. *The Journal of Chemical Physics* **2013**, *139*, 154105.

38. Bozkaya, U., Accurate Electron Affinities from the Extended Koopmans' Theorem Based on Orbital-Optimized Methods. *J Chem Theory Comput* **2014**, *10*, 2041-2048.

39. Yildiz, D.; Bozkaya, U., Assessment of the Extended Koopmans' Theorem for the Chemical Reactivity: Accurate Computations of Chemical Potentials, Chemical Hardnesses, and Electrophilicity Indices. *J Comput Chem* **2016**, *37*, 345-353.

40. Perdew, J. P.; Zunger, A., Self-Interaction Correction to Density-Functional Approximations for Many-Electron Systems. *Phys Rev B* **1981**, *23*, 5048-5079.

41. Perdew, J. P., Size-Consistency, Self-Interaction Correction, and Derivative Discontinuity in Density Functional Theory. In *Advances in Quantum Chemistry*, Per-Olov, L., Ed. Academic Press: 1990; Vol. Volume 21, pp 113-134.

42. Kim, M.-C.; Sim, E.; Burke, K., Communication: Avoiding Unbound Anions in Density Functional Calculations. *The Journal of Chemical Physics* **2011**, *134*, 171103.

43. Rösch, N.; Trickey, S. B., Comment on "Concerning the Applicability of Density Functional Methods to Atomic and Molecular Negative Ions" [J. Chem. Phys. 105, 862 (1996)]. *The Journal of Chemical Physics* **1997**, *106*, 8940-8941.

44. Janak, J. F., Proof That $\partial E/\partial N=E$ in Density-Functional Theory. *Phys Rev B* **1978**, *18*, 7165-7168.

45. Peach, M. J. G.; Teale, A. M.; Helgaker, T.; Tozer, D. J., Fractional Electron Loss in Approximate Dft and Hartree–Fock Theory. *J Chem Theory Comput* **2015**, *11*, 5262-5268.

46. Foster, M. E.; Wong, B. M., Nonempirically Tuned Range-Separated Dft Accurately Predicts Both Fundamental and Excitation Gaps in DNA and Rna Nucleobases. *J. Chem. Theory Comput.* **2012**, *8*, 2682-2687.

47. Wong, B. M.; Piacenza, M.; Sala, F. D., Absorption and Fluorescence Properties of Oligothiophene Biomarkers from Long-Range-Corrected Time-Dependent Density Functional Theory. *Physical Chemistry Chemical Physics* **2009**, *11*, 4498-4508.

48. Wong, B. M.; Cordaro, J. G., Coumarin Dyes for Dye-Sensitized Solar Cells: A Long-Range-Corrected Density Functional Study. *J Chem Phys* **2008**, *129*.

49. Wong, B. M.; Hsieh, T. H., Optoelectronic and Excitonic Properties of Oligoacenes: Substantial Improvements from Range-Separated Time-Dependent Density Functional Theory. *J Chem Theory Comput* **2010**, *6*, 3704-3712.

50. Raeber, A. E.; Wong, B. M., The Importance of Short- and Long-Range Exchange on Various Excited State Properties of DNA Monomers, Stacked Complexes, and Watson–Crick Pairs. *J Chem Theory Comput* **2015**, *11*, 2199-2209.

51. Richard, R. M.; Herbert, J. M., Time-Dependent Density-Functional Description of the 1la State in Polycyclic Aromatic Hydrocarbons: Charge-Transfer Character in Disguise? *J. Chem. Theory Comput.* **2011**, *7*, 1296-1306.

52. Kuritz, N.; Stein, T.; Baer, R.; Kronik, L., Charge-Transfer-Like Π→Π* Excitations in Time-Dependent Density Functional Theory: A Conundrum and Its Solution. *J. Chem. Theory Comput.* **2011**, *7*, 2408-2415.

53. Stein, T.; Eisenberg, H.; Kronik, L.; Baer, R., Fundamental Gaps in Finite Systems from Eigenvalues of a Generalized Kohn-Sham Method. *Phys Rev Lett* **2010**, *105*.

54. Stein, T.; Kronik, L.; Baer, R., Reliable Prediction of Charge Transfer Excitations in Molecular Complexes Using Time-Dependent Density Functional Theory. *J Am Chem Soc* **2009**, *131*, 2818-+.

55. Stein, T.; Kronik, L.; Baer, R., Prediction of Charge-Transfer Excitations in Coumarin-Based Dyes Using a Range-Separated Functional Tuned from First Principles. *J. Chem. Phys.* **2009**, *131*, 244119.

56. Kronik, L.; Stein, T.; Refaely-Abramson, S.; Baer, R., Excitation Gaps of Finite-Sized Systems from Optimally Tuned Range-Separated Hybrid Functionals. *J. Chem. Theory Comput.* **2012**, *8*, 1515-1531.

57. Stein, T.; Kronik, L.; Baer, R., Reliable Prediction of Charge Transfer Excitations in Molecular Complexes Using Time-Dependent Density Functional Theory. *J. Am. Chem. Soc.* **2009**, *131*, 2818-2820.

58. Jensen, F., Polarization Consistent Basis Sets. Iii. The Importance of Diffuse Functions. *The Journal of Chemical Physics* **2002**, *117*, 9234-9240.

59. Frisch, M. J., et al. *Gaussian 09*, Gaussian, Inc.: Wallingford, CT, USA, 2009.

60. Murray, C. W.; Handy, N. C.; Laming, G. J., Quadrature Schemes for Integrals of Density Functional Theory. *Mol Phys* **1993**, *78*, 997-1014.

61. Oviedo, M. B.; Ilawe, N. V.; Wong, B. M., Polarizabilities of Π-Conjugated Chains Revisited: Improved Results from Broken-Symmetry Range-Separated Dft and New Ccsd(T) Benchmarks. *J Chem Theory Comput* **2016**, *12*, 3593-3602.

62. Lee, C.; Yang, W.; Parr, R. G., Development of the Colle-Salvetti Correlation-Energy Formula into a Functional of the Electron Density. *Phys Rev B* **1988**, *37*, 785-789.

63. Medvedev, M. G.; Bushmarinov, I. S.; Sun, J.; Perdew, J. P.; Lyssenko, K. A., Density Functional Theory Is Straying from the Path toward the Exact Functional. *Science* **2017**, *355*, 49-52.

64. Pari, S.; Wang, I. A.; Liu, H.; Wong, B. M., Sulfate Radical Oxidation of Aromatic Contaminants: A Detailed Assessment of Density Functional Theory and High-Level Quantum Chemical Methods. *Environmental Science: Processes & Impacts* **2017**.

65. Jensen, F., Polarization Consistent Basis Sets. Iii. The Importance of Diffuse Functions. *J Chem Phys* **2002**, *117*, 9234-9240.

66. Kramida, A. R., Y.; Reader, J.; NIST ASD Team, Nist Atomic Spectra Database (Ver. 5.2). National Institute of Standards Technology: Gaithersburg, MD, 2014.

67. Rienstra-Kiracofe, J. C.; Tschumper, G. S.; Schaefer, H. F., 3rd; Nandi, S.; Ellison, G. B., Atomic and Molecular Electron Affinities: Photoelectron Experiments and Theoretical Computations. *Chem Rev* **2002**, *102*, 231-82.

68. Auffinger, P.; Hays, F. A.; Westhof, E.; Ho, P. S., Halogen Bonds in Biological Molecules. *P Natl Acad Sci USA* **2004**, *101*, 16789-16794.

69. Hardegger, L. A., et al., Systematic Investigation of Halogen Bonding in Protein-Ligand Interactions. *Angew Chem Int Edit* **2011**, *50*, 314-318.

70. Metrangolo, P.; Resnati, G., Halogen Bonding: A Paradigm in Supramolecular Chemistry. *Chem-Eur J* **2001**, *7*, 2511-2519.

71. Meyer, F.; Dubois, P., Halogen Bonding at Work: Recent Applications in Synthetic Chemistry and Materials Science. *Crystengcomm* **2013**, *15*, 3058-3071.

72. Lu, Y. X.; Zou, J. W.; Wang, Y. H.; Jiang, Y. J.; Yu, Q. S., Ab Initio Investigation of the Complexes between Bromobenzene and Several Electron Donors: Some Insights into the Magnitude and Nature of Halogen Bonding Interactions. *J Phys Chem A* **2007**, *111*, 10781-10788.

73. Metrangolo, P.; Neukirch, H.; Pilati, T.; Resnati, G., Halogen Bonding Based Recognition Processes: A World Parallel to Hydrogen Bonding. *Accounts Chem Res* **2005**, *38*, 386-395.

74. Murrayrust, P.; Stallings, W. C.; Monti, C. T.; Preston, R. K.; Glusker, J. P., Intermolecular Interactions of the C-F Bond - the Crystallographic Environment of Fluorinated Carboxylic-Acids and Related Structures. *J Am Chem Soc* **1983**, *105*, 3206-3214.

75. Murrayrust, P.; Motherwell, W. D. S., Computer Retrieval and Analysis of Molecular-Geometry .4. Inter-Molecular Interactions. *J Am Chem Soc* **1979**, *101*, 4374-4376.

76. Ramasubbu, N.; Parthasarathy, R.; Murrayrust, P., Angular Preferences of Intermolecular Forces around Halogen Centers - Preferred Directions of Approach of Electrophiles and Nucleophiles around the Carbon Halogen Bond. *J Am Chem Soc* **1986**, *108*, 4308-4314.

77. Masunov, A. E.; Zorkii, P. M., Donor-Acceptor Nature of Specific Nonbonded Interactions of Sulfur and Halogen Atoms - Influence on the Geometry and Packing of Molecules. *J Struct Chem+* **1992**, *33*, 423-435.

78. Lommerse, J. P. M.; Stone, A. J.; Taylor, R.; Allen, F. H., The Nature and Geometry of Intermolecular Interactions between Halogens and Oxygen or Nitrogen. *J Am Chem Soc* **1996**, *118*, 3108-3116.

79. Politzer, P.; Murray, J. S.; Concha, M. C., Sigma-Hole Bonding between Like Atoms; a Fallacy of Atomic Charges. *J Mol Model* **2008**, *14*, 659-665.

80. Politzer, P.; Murray, J. S.; Clark, T., Halogen Bonding: An Electrostatically-Driven Highly Directional Noncovalent Interaction. *Phys Chem Chem Phys* **2010**, *12*, 7748-7757.

81. Clark, T.; Hennemann, M.; Murray, J. S.; Politzer, P., Halogen Bonding: The Sigma-Hole. *J Mol Model* **2007**, *13*, 291-296.

82. Politzer, P.; Lane, P.; Concha, M. C.; Ma, Y. G.; Murray, J. S., An Overview of Halogen Bonding. *J Mol Model* **2007**, *13*, 305-311.

83. Metrangolo, P.; Murray, J. S.; Pilati, T.; Politzer, P.; Resnati, G.; Terraneo, G., The Fluorine Atom as a Halogen Bond Donor, Viz. A Positive Site. *Crystengcomm* **2011**, *13*, 6593-6596.

84. Legon, A. C., The Halogen Bond: An Interim Perspective. *Phys Chem Chem Phys* **2010**, *12*, 7736-7747.

85. Kozuch, S.; Martin, J. M. L., Halogen Bonds: Benchmarks and Theoretical Analysis. *J Chem Theory Comput* **2013**, *9*, 1918-1931.

86. Janak, J. F., Proof That Delta-E-Delta-Ni=Epsilon-I in Density-Functional Theory. *Phys Rev B* **1978**, *18*, 7165-7168.

87. Anderson, L. N.; Oviedo, M. B.; Wong, B. M., Accurate Electron Affinities and Orbital Energies of Anions from a Nonempirically Tuned Range-Separated Density Functional Theory Approach. *J Chem Theory Comput* **2017**, *13*, 1656-1666.

88. Tawada, Y.; Tsuneda, T.; Yanagisawa, S.; Yanai, T.; Hirao, K., A Long-Range-Corrected Time-Dependent Density Functional Theory. *J. Chem. Phys.* **2004**, *120*, 8425-8433.

89. Toulouse, J.; Colonna, F.; Savin, A., Long-Range–Short-Range Separation of the Electron-Electron Interaction in Density-Functional Theory. *Phys. Rev. A* **2004**, *70*, 062505.

90. Tawada, Y.; Tsuneda, T.; Yanagisawa, S.; Yanai, T.; Hirao, K., A Long-Range-Corrected Time-Dependent Density Functional Theory. *J Chem Phys* **2004**, *120*, 8425-8433.

91. Toulouse, J.; Colonna, F.; Savin, A., Long-Range-Short-Range Separation of the Electron-Electron Interaction in Density-Functional Theory. *Phys Rev A* **2004**, *70*.

92. Richard, R. M.; Herbert, J. M., Time-Dependent Density-Functional Description of the L-1(a) State in Polycyclic Aromatic Hydrocarbons: Charge-Transfer Character in Disguise? *J Chem Theory Comput* **2011**, *7*, 1296-1306.

93. Kuritz, N.; Stein, T.; Baer, R.; Kronik, L., Charge-Transfer-Like Pi(->)Pi* Excitations in Time-Dependent Density Functional Theory: A Conundrum and Its Solution. *J Chem Theory Comput* **2011**, *7*, 2408-2415.

94. Raeber, A. E.; Wong, B. M., The Importance of Short- and Long-Range Exchange on Various Excited State Properties of DNA Monomers, Stacked Complexes, and Watson-Crick Pairs. *J Chem Theory Comput* **2015**, *11*, 2199-2209.

95. Rohrdanz, M. A.; Martins, K. M.; Herbert, J. M., A Long-Range-Corrected Density Functional That Performs Well for Both Ground-State Properties and Time-Dependent Density Functional Theory Excitation Energies, Including Charge-Transfer Excited States. *J. Chem. Phys.* **2009**, *130*, 054112.

96. Refaely-Abramson, S.; Sharifzadeh, S.; Govind, N.; Autschbach, J.; Neaton, J. B.; Baer, R.; Kronik, L., Quasiparticle Spectra from a Nonempirical Optimally Tuned Range-Separated Hybrid Density Functional. *Phys. Rev. Lett.* **2012**, *109*, 226405.

97. Egger, D. A.; Weismann, S.; Refaely-Abramson, S.; Sharifzadeh, S.; Dauth, M.; Baer, R.; Kummel, S.; Neaton, J. B.; Zojer, E.; Kronik, L., Outer-Valence Electron

Spectra of Prototypical Aromatic Heterocycles from an Optimally-Tuned Range-Separated Hybrid Functional. *J. Chem. Theory Comput.* **2014**.

98. Srebro, M.; Autschbach, J., Does a Molecule-Specific Density Functional Give an Accurate Electron Density? The Challenging Case of the Cucl Electric Field Gradient. *J. Phys. Chem. Lett.* **2012**, *3*, 576-581.

99. Karolewski, A.; Kronik, L.; Kümmel, S., Using Optimally Tuned Range Separated Hybrid Functionals in Ground-State Calculations: Consequences and Caveats. *The Journal of Chemical Physics* **2013**, *138*, 204115.

100. Grimme, S.; Antony, J.; Ehrlich, S.; Krieg, H., A Consistent and Accurate Ab Initio Parametrization of Density Functional Dispersion Correction (Dft-D) for the 94 Elements H-Pu. *The Journal of Chemical Physics* **2010**, *132*, 154104.

101. Grimme, S.; Ehrlich, S.; Goerigk, L., Effect of the Damping Function in Dispersion Corrected Density Functional Theory. *J Comput Chem* **2011**, *32*, 1456-1465.

102. Becke, A. D.; Johnson, E. R., A Density-Functional Model of the Dispersion Interaction. *J. Chem. Phys.* **2005**, *123*, 154101.

103. Johnson, E. R.; Becke, A. D., A Post-Hartree–Fock Model of Intermolecular Interactions. *J. Chem. Phys.* **2005**, *123*, 024101.

104. Johnson, E. R.; Becke, A. D., A Post-Hartree-Fock Model of Intermolecular Interactions: Inclusion of Higher-Order Corrections. *J. Chem. Phys.* **2006**, *124*, 174104.

105. Gaussian 09, R. B., M. J. Frisch, G. W. Trucks, H. B. Schlegel, G. E. Scuseria, M. A. Robb, J. R. Cheeseman, G. Scalmani, V. Barone, B. Mennucci, G. A. Petersson, H. Nakatsuji, M. Caricato, X. Li, H. P. Hratchian, A. F. Izmaylov, J. Bloino, G. Zheng, J. L. Sonnenberg, M. Hada, M. Ehara, K.Toyota, R. Fukuda, J. Hasegawa, M. Ishida, T. Nakajima,Y. Honda, O. Kitao, H. Nakai, T. Vreven, J. A. Montgomery, Jr.,J. E. Peralta, F. Ogliaro, M. Bearpark, J. J. Heyd, E. Brothers, K. N. Kudin, V. N. Staroverov, T. Keith, R. Kobayashi, J. Normand, K. Raghavachari, A. Rendell, J. C. Burant, S. S. Iyengar, J. Tomasi,M. Cossi, N. Rega, J. M. Millam, M. Klene, J. E. Knox, J. B. Cross, V. Bakken, C. Adamo, J. Jaramillo, R. Gomperts, R. E. Stratmann, O. Yazyev, A. J. Austin, R. Cammi, C. Pomelli, J. W. Ochterski, R. L. Martin, K. Morokuma, V. G. Zakrzewski, G. A. Voth, P. Salvador, J. J. Dannenberg, S. Dapprich, A. D. Daniels, O. Farkas, J. B. Foresman, J. V. Ortiz, J. Cioslowski, and D. J. Fox, Gaussian, Inc., Wallingford CT, 2010. , **2010**.

106. Grimme, S. A., J.; Ehrlich, S.; Krieg, H. Dft-D3 - a Dispersion Correction for Density Functionals, Hartree-Fock and Semi-Empirical Quantum Chemical Methods. http://www.thch.uni-bonn.de/tc/dftd3.

107. Web of Science. http://apps.webofknowledge.com (accessed accessed July 8, 2017).

Appendix A

Supporting Information for Chapter 1:

Plot of $\langle R^2 \rangle$ vs. $1/\mu$ obtained with the smaller aug-pc-2 basis, total energies for all three rows of elements (H – Ar) of the periodic table calculated at the HF, BLYP, B3LYP, BHHLYP, and LC-BLYP levels of theory with the aug-pc-2 and aug-pc-∞ basis sets, and uncontracted aug-pc-2 and aug-pc-∞ basis sets for all three rows of elements (H – Ar) of the periodic table.

(See attachment)

Appendix B

Supporting Information for Chapter 2:

Detailed, color-coded comparison of inconsistencies within the XB51 set, absolute errors in the dissociation energy predicted by the non-empirically tuned LC-ωPBE functional for halogen-bonding dimers within the XB18 and XB51 benchmark set, and total electronic energies and dissociation energies for all 69 dimers in the XB18 and XB51 sets.

(See attachment)